ERA report series

12 Atmospheric conservation properties in ERA-Interim

P. Berrisford, P. Kållberg[1], S. Kobayashi[2], D. Dee, S. Uppala, A. J. Simmons, P. Poli and H. Sato

[1]SMHI, Norrkoping, Sweden [2]JMA, Tokyo, Japan

Series: ECMWF ERA Report

A full list of ECMWF Publications can be found on our web site under:
http://www.ecmwf.int/publications/

Contact: library@ecmwf.int

© Copyright 2011

European Centre for Medium Range Weather Forecasts
Shinfield Park, Reading, Berkshire RG2 9AX, England

Literary and scientific copyrights belong to ECMWF and are reserved in all countries. This publication is not to be reprinted or translated in whole or in part without the written permission of the Director. Appropriate non-commercial use will normally be granted under the condition that reference is made to ECMWF.

The information within this publication is given in good faith and considered to be true, but ECMWF accepts no liability for error, omission and for loss or damage arising from its use.

ERA report series No. 12

Atmospheric conservation properties in ERA-Interim

P. Berrisford, P. Kållberg[1], S. Kobayashi[2], D. Dee, S. Uppala, A. J. Simmons, P. Poli and H. Sato

[1] SMHI, Norrkoping, Sweden

[2] JMA, Tokyo, Japan

This paper has been accepted for publication in Quarterly Journal of the Royal Meteorological Society

Abstract

We study the global atmospheric budgets of mass, moisture, energy and angular momentum in the latest reanalysis from The European Centre for Medium-Range Weather Forecasts (ECMWF), ERA-Interim, for the period 1989-2008 and compare with ERA-40. Most of the measures we use indicate that the ERA-Interim reanalysis is superior in quality to ERA-40. In ERA-Interim the standard deviation of the monthly mean global dry mass of 0.7 kgm^{-2} (0.007%) is slightly worse than in ERA-40, and long time scale variations in dry mass originate predominately in the surface pressure field. The divergent winds are improved in ERA-Interim: the global standard deviation of the time averaged dry mass budget residual is 10 $kgm^{-2}day^{-1}$ and the quality of the cross equatorial mass fluxes is improved. The temporal variations in the global evaporation minus precipitation (*E-P*) are too large but the global moisture budget residual is 0.003 $kgm^{-2}day^{-1}$ with a spatial standard deviation of 0.3 $kgm^{-2}day^{-1}$. Both the *E-P* over ocean and *P-E* over land are about 15% larger than the 1.1 Tgs^{-1} transport of water from ocean to land. The top of atmosphere (TOA) net energy losses are improved, with a value of 1 Wm^{-2} but the meridional gradient of the TOA net energy flux is smaller than that from the Clouds and the Earth's Radiant Energy System (CERES) data. At the surface the global energy losses are worse, with a value of 7 Wm^{-2}. Over land however, the energy loss is only 0.5 Wm^{-2}. The downwelling thermal radiation at the surface in ERA-Interim of 341 Wm^{-2} is towards the higher end of previous estimates. The global mass adjusted energy budget residual is 8 Wm^{-2} with a spatial standard deviation of 11 Wm^{-2} and the mass adjusted atmospheric energy transport from low to high latitudes (the sum for the two hemispheres) is 9.5 PW.

1 Introduction

Reanalysis is a process whereby past observations of the atmosphere, which have ideally undergone modern data quality checks and re-processing, are reanalysed using a state of the art numerical weather prediction (NWP) analysis and forecast system. This procedure produces the best possible analyses at that time, with the best time consistency, from a given NWP centre. However, because the analysis and forecast system is continually changing, with a view to improving weather forecasts, the reanalysis procedure needs to be repeated every few years in order to benefit from the latest enhancements to the system.

The European Centre for Medium-Range Weather Forecasts (ECMWF) have produced two major reanalyses, ERA-15 (Gibson *et al*. 1997) and ERA-40 (Uppala *et al*. 2005). These reanalyses, and others, provide a means of viewing the global circulation of the atmosphere, e g Kållberg *et al*. (2005), and numerous studies have gained insight into the workings of that circulation by using reanalysis data. However, ERA-40 (and ERA-15 before it) did suffer from various deficiencies (Uppala *et al*. 2005). ERA-Interim (Simmons *et al*. 2007, Uppala et al. 2008, Dee et al. 2011) was instigated to address some of the problems seen in ERA-40, in the satellite years in particular, and runs from 1989 to the present. It will continue in near real time until a replacement can be produced. Simmons et al. (2007) and Dee et al. (2011) discuss the improvements made to the ERA-Interim system and observations. The major improvements over ERA-40 are the use of 4D variational assimilation (4D-Var), variational bias correction (VarBC) of satellite radiances (Dee and Uppala 2009), higher horizontal resolution, a new humidity analysis and improved model physics and the homogenisation of radiosonde temperature observations (Haimberger 2007).

Here, we examine the properties of atmospheric mass, moisture, energy and angular momentum, mostly for the global domain, which are variables that are governed by simple physical constraints. Neither the ERA forecast nor assimilation systems are designed to satisfy these physical constraints so the degree to which the reanalyses conform to these constraints provides one measure of the quality of

the data. Mainly, we compare with ERA-40 but some comparison is also made with the reanalysis of the Japanese Meteorological Agency (JMA) and the Japanese Central Research Institute of the Electric Power Industry (Onogi et al 2007) and its continuation into near real time, JRA-25, the NCEP/DOE AMIP-II reanalysis, NRA2, (Kistler et al 2001), the Global Precipitation Climatology (GPCP) precipitation data (Adler et al. 2003) and the Clouds and the Earth's Radiant Energy System (CERES) radiative fluxes.

This paper is organised as follows. Section 2 below describes the data used in this study and then Sections 3, 4 and 5 examine the properties of mass and moisture, energy and angular momentum respectively. Section 6 presents the summary and conclusions.

2 Data

This study mainly uses monthly averages for 1989-2008. ERA data is taken at full horizontal resolution from MARS (the ECMWF data archive) on all 60 model levels and at the surface. The horizontal model grids are N128 and N80 reduced Gaussian grids, giving grid lengths of approximately 80 and 125 km, for ERA-Interim and ERA-40 respectively. Where necessary, spectral data are transformed to the same grids. Vertical integration is performed on the model level fields and the results for ERA-Interim and ERA-40 are archived in MARS. More information on the content of the ERA-Interim and ERA-40 archives can be found in Berrisford et al. (2009) and Kållberg et al. (2004). The data in most of the global maps shown here have been smoothed using a Hoskins type spectral filter (Sardeshmukh and Hoskins 1984) with an attenuation of 0.1 at wavenumber 106. Apart from removing the small scale structure this enables the comparison of the spatial standard deviation between data of differing resolutions. Mass adjustment of the divergence of fluxes is carried out, where necessary, using the procedure given by Chiodo and Haimberger 2010. Note that this procedure introduces a non-zero global mean to the divergence. All linear trends shown here are computed from the anomalies from the mean annual cycle, because otherwise the trends might be contaminated with that cycle.

Some of the fields that we examine are analysed fields, which are constrained by observations, but others such as the surface and top of the atmosphere (TOA) radiative fluxes and surface turbulent fluxes can not be analysed so are estimated from short-range forecasts. The latter are model produced and not directly constrained by observations and so are inherently less reliable than analysed fields. All ERA fluxes used here are from the twice daily forecasts (at 00 and 12 UTC) and are accumulated from the first twelve hours of the forecast. All vertical fluxes from MARS are defined to be positive downwards. We confine this study to the first 20 years of ERA-Interim, from 1989 to 2008, including the overlapping 13 year period in ERA-40, from 1989 to 2001.

Monthly mean JRA-25 analyses and six hour forecasts are taken on a regular N80 Gaussian grid, monthly mean NRA2 analyses and six hour forecasts are taken on a 2.5°x2.5° latitude/longitude or regular N47 Gaussian grid. Monthly mean fields are taken from GPCPv2.1 and CERES data on a 2.5°x2.5° and 1°x1° latitude/longitude grid respectively.

3 Mass and moisture

Mass is a very basic property of the atmosphere and as such warrants investigation when considering the quality of a reanalysis dataset. Here, we investigate the vertically integrated quantities of mass and water vapour and their difference, dry mass. The effects of water in other phases are small compared to those of water vapour and so are neglected (Trenberth and Smith 2005).

For an atmospheric column, the mass, m, total column water vapour, TCWV, and dry mass, m_d , are computed from the pressure, p, and specific humidity, q, assuming a spherical earth and uniform gravitational acceleration, g, so that

$$m = \frac{1}{g}\int_0^1 \frac{\partial p}{\partial \eta} d\eta \tag{1}$$

$$TCWV = \frac{1}{g}\int_0^1 q\frac{\partial p}{\partial \eta} d\eta \tag{2}$$

$$m_d = \frac{1}{g}\int_0^1 (1-q)\frac{\partial p}{\partial \eta} d\eta \tag{3}$$

where η is the hybrid coordinate (Simmons and Burridge 1981) and the masses are measured in kgm^{-2}. The real mass of the atmosphere is estimated to be 0.25% larger than that given by (1) due to the widening with height of air columns in the spherical geometry of the earth (Bannon et al. 1997). The effects of the spatial variation of g and the non-spherical shape of the earth were investigated by Trenberth and Guillemot (1994) and, to a good approximation, the total atmospheric mass of the earth implied by (1) and expressed in kg, should be increased by 0.43% (Trenberth and Smith 2005).

The evolution of the masses is governed by the vertically integrated continuity equations for m, $TCWV$ and m_d, which link the divergence of the mass fluxes with the atmospheric mass tendencies in the following way

$$\frac{\partial m}{\partial t} = -\underline{\nabla}\cdot\frac{1}{g}\int_0^1 \underline{v}\frac{\partial p}{\partial \eta} d\eta + E - P \tag{4}$$

$$\frac{\partial TCWV}{\partial t} = -\underline{\nabla}\cdot\frac{1}{g}\int_0^1 \underline{v}q\frac{\partial p}{\partial \eta} d\eta + E - P \tag{5}$$

$$\frac{\partial m_d}{\partial t} = -\underline{\nabla}\cdot\frac{1}{g}\int_0^1 \underline{v}(1-q)\frac{\partial p}{\partial \eta} d\eta \tag{6}$$

where $\underline{v}$ is the horizontal vector wind, $\underline{\nabla}$ is the "horizontal" gradient operator, E is evaporation and P is precipitation. Note that (4) and (5) have the same source term (E-P, defined to be positive into the atmosphere), though this is not included in the ERA forecast model's continuity equation (4). For analyses, however, the assimilation of observations should introduce the effects of this source term.

3.1 Global mass and moisture

For the case of global masses, the divergence terms are zero, so that (4) and (5) state that the global mass and water tendencies are governed by the global average of the same source term, E-P, while (6) states that the global dry mass tendency has no source term. Hence, the variations in global mass and $TCWV$ should be well correlated and the global mass of dry air, the difference between the two, should be conserved, making it a very basic property of the atmosphere. In reality, the dry mass changes for

various reasons not taken account of in (6), the largest changes currently being due to the burning of fossil fuels. However, the effect of the latter is of order 0.1 kgm^{-2} (Trenberth and Smith 2005) which is not detectable with current reanalyses, see below. It would be possible to maintain the global mass at a fixed value in the ERA forecast model. However, it is not possible to do so in the data assimilation system. Furthermore, we look to reanalyses to provide us with estimates of the global mass. So in ERA the mass is determined by the system and, as previously noted, the degree to which the system conserves the mass is one measure of the quality of the data.

First we look at the mean annual cycle in the global mass and *TCWV*, where both quantities reach their maximum in July or August and minimum in December or January (Table 1). In ERA-Interim for the 20 year period 1989-2008 the range (maximum-minimum) of the annual cycle in *TCWV* of 3.1 kgm^{-2} is 15 % larger than that in mass of 2.7 kgm^{-2}. In ERA-40 for the 13 year period 1989-2001, the range in *TCWV* of 3.2 kgm^{-2} is 28 % larger than that in mass, a similar result to that found by Trenberth and Smith (2005). Consequently, the range of the mean annual cycle in dry mass is smaller in ERA-Interim than in ERA-40, particularly for the period 1989-2001 when it is 0.4 kgm^{-2} for the former and 0.8 kgm^{-2} for the latter.

	Mass	**Mass**	**Mass**	***TCWV***	***TCWV***	***TCWV***	**Dry mass**	**Dry mass**	**Dry mass**
	EI 20	**EI 13**	**E4 13**	**EI 20**	**EI 13**	**E4 13**	**EI 20**	**EI 13**	**E4 13**
Jan	48.3	48.2	48.0	23.1	23.0	23.9	25.2	25.2	24.1
Feb	48.6	48.6	48.2	23.4	23.3	24.1	25.3	25.2	24.1
Mar	48.9	48.9	48.5	23.7	23.7	24.6	25.3	25.2	23.9
Apr	49.2	49.2	48.8	24.1	24.1	25.1	25.1	25.2	23.7
May	49.4	49.6	49.2	24.5	24.6	25.7	24.8	25.0	23.5
Jun	49.9	50.0	49.8	25.3	25.2	26.3	24.6	24.8	23.5
Jul	50.8	50.9	50.5	26.1	26.1	27.1	24.7	24.8	23.4
Aug	50.7	50.8	50.5	26.0	26.0	27.0	24.8	24.9	23.6
Sep	49.8	49.8	49.7	24.9	24.8	25.7	24.9	25.0	23.9
Oct	48.8	48.8	48.8	23.9	23.8	24.7	25.0	25.1	24.1
Nov	48.3	48.3	48.3	23.2	23.2	24.1	25.1	25.1	24.2
Dec	48.1	48.1	48.1	23.0	23.0	24.0	25.1	25.1	24.1
Ann	49.2	49.3	49.0	24.3	24.2	25.2	25.0	25.0	23.8
Max-min	2.7	2.8	2.5	3.1	3.1	3.2	0.7	0.4	0.8

Table 1: Mean annual cycle of global mass, TCWV and dry mass in ERA-Interim (EI) and ERA-40 (E4) for the 20 year period 1989-2008 and 13 year period 1989-2001. For mass and dry mass the units are kgm^{-2} -10000 while for TCWV they are kgm^{-2}.

The monthly mean time series of analysed global mass, *TCWV* and dry mass (Figure 1) show that indeed, the variations in the analysed mass and *TCWV* are larger than those in dry mass, both for ERA-Interim and ERA-40, and this is measured by the standard deviations of the three quantities (Table 2) from their annual climates (Table 1). The standard deviation from the annual climates of global dry mass in ERA-Interim for the years 1989-2008 is 0.74 kgm^{-2} (0.073 hPa) or 0.0074% and in ERA-40 for 1989-2001 it is 0.58 kgm^{-2} (0.057 hPa) or 0.0058%. The free running ERA-Interim model, in the absence of the assimilation of observations, is estimated to gain mass by about 0.3% per year (Agathe Untch pers. comm. 2009) and so the analyses conserve global dry mass much better than does the forecast model. This is due to the plentiful supply, and good treatment, of high quality observations.

Although as previously mentioned, the standard deviations of global dry mass are smaller than those for mass and *TCWV*, the values are at most only 50% smaller (Table 2), indicating that the variations in dry mass are not negligible compared to those in mass and *TCWV*. The dry mass in ERA-Interim increases from a low point of 10023.7 kgm^{-2} in 1990 to a maximum of 10026.6 kgm^{-2} in 2000, then decreases to a low point of 10023.6 kgm^{-2} in 2007 (Figure 1). The behaviour in ERA-40 is different, with a minimum of 10022.6 kgm^{-2} in 1995, a maximum of 10025.4 kgm^{-2} in 1999 and returning to more usual values by 2001. The magnitude of these variations is similar in ERA-Interim and ERA-40 (peak to peak values of 2.9 kgm^{-2} and 2.8 kgm^{-2} respectively) but the standard deviation in ERA-Interim is nearly 30% larger than that in ERA-40. This disparity occurs because although the dry mass in ERA-40 appears to suffer larger variations than ERA-Interim on month to month time scales, e.g. in the latter half of 1998, that in ERA-Interim varies more on longer time scales of years. There is no known physical reason why the dry mass in ERA-Interim should exhibit such long time scale variations, or why it exhibits short time scale variations in ERA-40, so it is likely that these variations are spurious.

The spurious variations in dry mass are due to problems either in the mass, *TCWV* or both. For *TCWV*, both the standard deviation from the mean annual cycle and the linear trends are considerably smaller than those for mass and dry mass and, for ERA-Interim in particular, those for dry mass are similar to those for mass (Figure 2 and Tables 2 and 3). This indicates for ERA-Interim in particular, that the spurious variations in dry mass arise primarily from variations in the mass that are absent from the *TCWV*. Although after the eruption of Mount Pinatubo in 1991 in particular, the *TCWV* is larger in ERA-40 than in ERA-Interim (Figure 1b) (Uppala et al. 2005), there are only relatively small differences in the deviations from the mean annual cycle for TCWV in ERA-40 and ERA-Interim (Figure 2b). The *TCWV* anomaly in ERA-Interim is positive for the period 1989-1991, but then shifts by about 1 kgm^{-2} to negative values. Apart from the ENSO period of 1997/98 the negative values last until 2001, from when there is a gradual increase over time. The negative shift is associated with an increase in SSM/I satellite observations in 1992 which gradually decrease from 2006 onwards. In ERA-Interim, these observations were not treated correctly, leading to a decrease in *TCWV* and precipitation (Dee et al. 2011). For most of the period of this negative shift, the *TCWV* anomaly in ERA-40 is larger than in ERA-Interim, particularly during and after the ENSO event. This negative shift of *TCWV* in ERA-Interim must be a contributory factor to the spurious variations in dry mass, but the magnitude of the shift is not large enough to completely explain those variations.

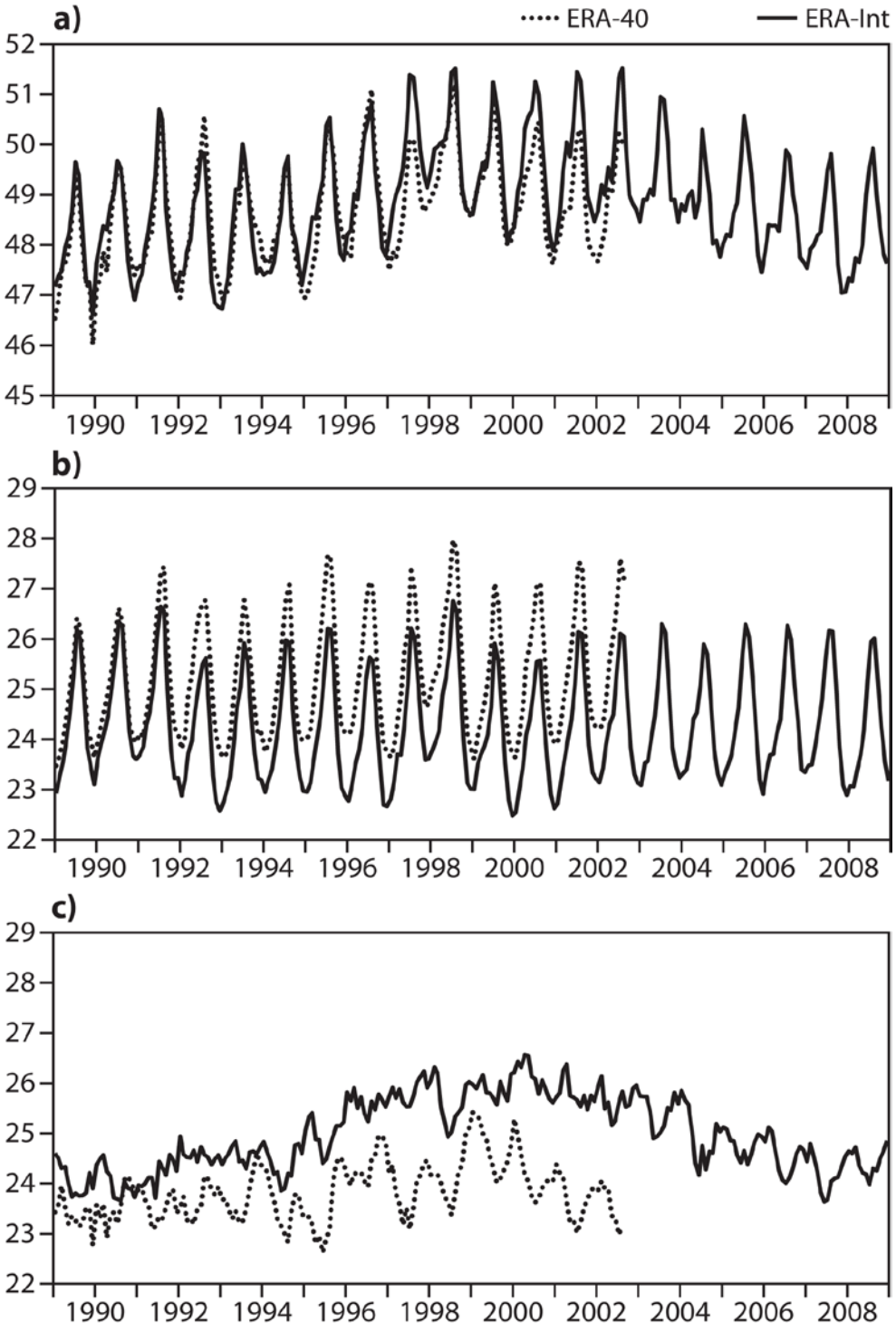

Figure 1: Vertically integrated global monthly mean time series from 1989 to 2008 for ERA-Interim (solid) and ERA-40 (dashed) of a) mass, b) TCWV and c) dry mass. The units are kgm^{-2} - 10000 for a) and c) and kgm^{-2} for b).

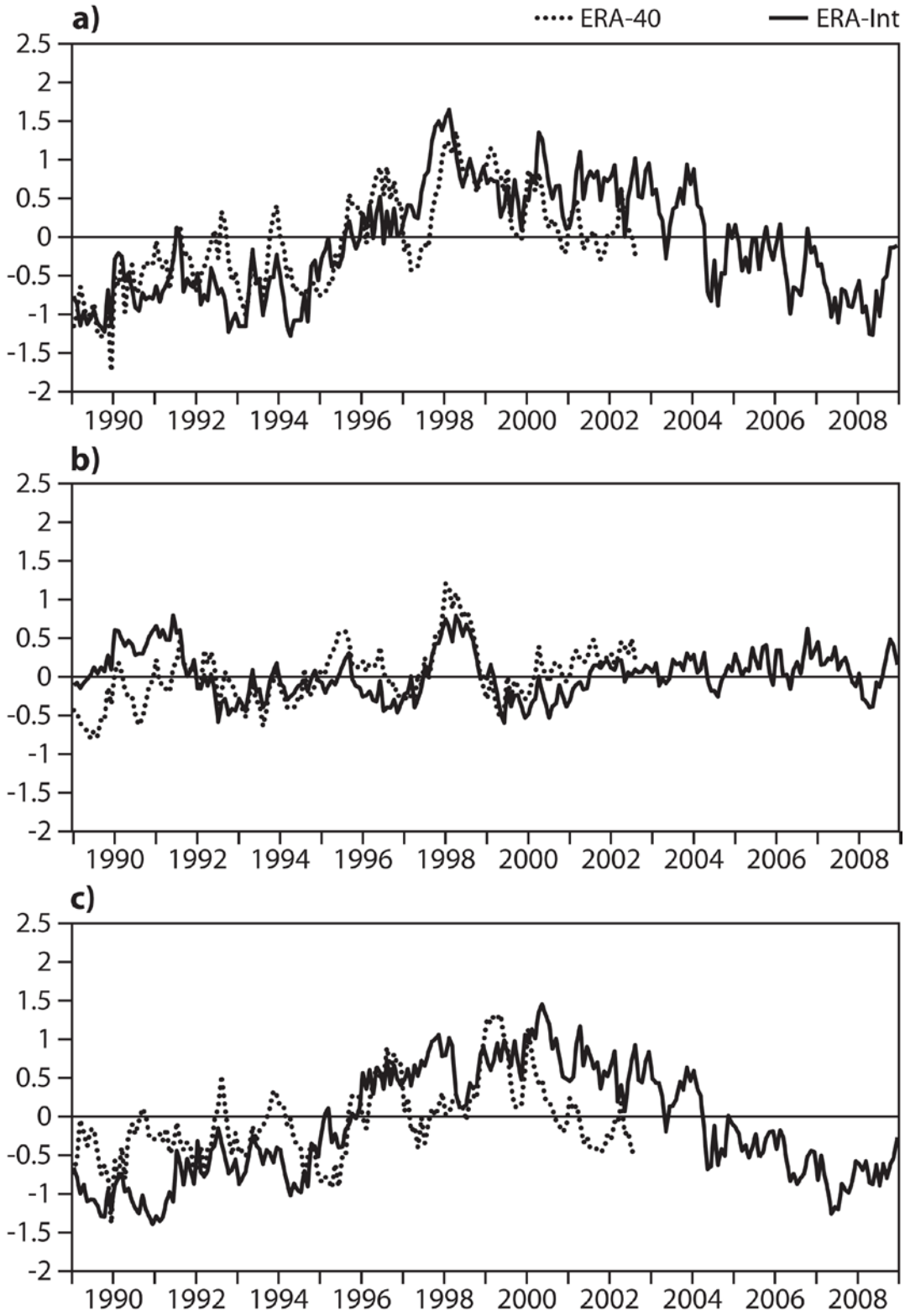

Figure 2: Vertically integrated global monthly mean time series anomalies from 1989 to 2008 for ERA-Interim (solid) and ERA-40 (dashed) of a) mass, b) TCWV and c) dry mass. The units are kgm^{-2} and the reference period is 1989-2001.

	Mass	*TCWV*	Dry mass
EI 20	1.12 (0.70)	1.08 (0.30)	0.74 (0.72)
EI 13	1.20 (0.75)	1.11 (0.33)	0.80 (0.78)
E4 13	1.07 (0.63)	1.17 (0.38)	0.58 (0.50)

Table 2: Standard deviation of global mass, TCWV and dry mass from the annual climate (the values in parentheses are standard deviations from the mean annual cycle) in ERA-Interim (EI) and ERA-40 (E4) for the 20 year period 1989-2008 and 13 year period 1989-2001. The units are kgm^{-2}.

	Mass	*TCWV*	Dry mass
EI 20	0.29	0.01	0.28
EI 13	1.65	-0.23	1.88
E4 13	1.09	0.44	0.65

Table 3: Linear trend for global mass, TCWV and dry mass in ERA-Interim (EI) and ERA-40 (E4) for the 20 year period 1989-2008 and 13 year period 1989-2001. The units are kgm^{-2}decade^{-1}.

For mass there is generally a good agreement between ERA-Interim and ERA-40 up until 1999 (Figure 1). However, there are some notable exceptions to this agreement. For example, the boreal summertime peak in ERA-Interim in 1997 is larger than that in ERA-40 while the opposite is true in 1992 and 1996. Both ERA-Interim and ERA-40 exhibit an increase in mass (and dry mass) during the mid 1990s (Figures 1a and 2a), culminating in the dramatic rise in mass and *TCWV* during 1997 associated with the El Niño event. During 2000, however, the mass (and dry mass) in ERA-40 decreases (Figure 1a) whereas that in ERA-Interim does not, and the anomaly remains positive until 2004 (Figure 2a).

It seems likely that the spurious long time scale variations of dry mass seen in ERA-Interim in particular, are, for the most part, due to spurious variations in the mass (surface pressure) field, although there is a contribution from the *TCWV*. The rise in mass and dry mass during the mid 1990s is curious but occurs in ERA-40 too (and in JRA-25). The elevated levels of mass and dry mass from 2000 in ERA-Interim are in disagreement with ERA-40 and although the source of this problem is unknown, it could be related in part to the new surface pressure bias correction scheme in ERA-Interim (Simmons 2007).

The global budgets also illustrate the degree to which the dry mass is conserved. The time series of the tendencies (calculated from the analysed values at the beginning of each month) of global mass and *TCWV* are reasonably well matched, having a standard deviation of 0.02-0.03 kgm^{-2}day^{-1} (Figures 3a and b). The standard deviation for the dry mass tendency is 0.015 and 0.023 kgm^{-2}day^{-1} for ERA-Interim and ERA-40 respectively (Figure 3c). While this tendency is not zero, as it would be if global dry mass was perfectly conserved, it is smaller than the tendencies of mass and *TCWV*. The tendencies of global mass and *TCWV* should be equal to the source, *E-P* (Figure 3d). However, the standard deviation for the latter is 0.08 kgm^{-2}day^{-1} for ERA-Interim and the pattern is quite different to that for the tendencies. Also, there are long periods when *E-P* is predominantly negative (1989-1996) and periods when it is positive (1998-2006). These shifts are related to changes in the observing system, such as the satellite measurements of *TCWV* from SSM/I (Dee et al. 2011). Clearly, the relationship

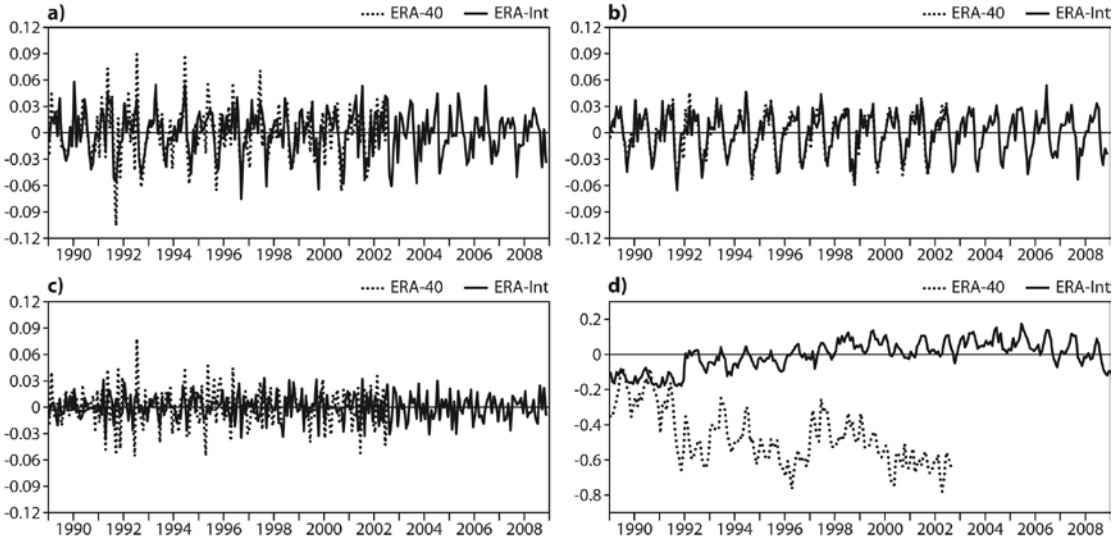

Figure 3: Vertically integrated global monthly mean time series from 1989 to 2008 for ERA-Interim (solid) and ERA-40 (dashed) of a) mass tendency, b) TCWV tendency, c) dry mass tendency and d) E-P (defined to be positive upwards into the atmosphere). The units are kgm^{-2}day^{-1}.

between the budget terms depends crucially on the period considered. Although the agreement between the global tendencies of mass and *TCWV* and *E-P* is not very good in ERA-Interim, it is still much better than for ERA-40 where *E-P* is far too negative and has a standard deviation of 0.16 kgm^{-2}day^{-1}, a problem which is related to the overactive hydrological cycle in ERA-40 (Uppala et al. 2005).

3.2 Hemispheric dry mass budgets

It has long been known that one of the greatest sources of uncertainty in atmospheric analyses originates in the divergent wind (Boer and Sargent 1985) and this problem has continued into more recent times (Graversen *et al*. 2007). Equations (4) – (6) link the tendencies of the mass fields with divergent mass fluxes. In forecasting models, erroneous divergent winds and mass fluxes lead to spurious surface pressure tendencies. In diagnostics, a further source of error is poor temporal sampling of the mass fluxes (Haimberger *et al.* 2001). Here, the mass fluxes are calculated from the four times daily analysed instantaneous values and so are not truly representative of the month as a whole - each instantaneous value of the vertically integrated mass flux divergence represents the column mass tendency at only one time step in the model.

Using reanalysis data we can use the tendencies of the mass fields, which are not so problematic to analyse as the divergent wind, to assess the quality of the divergent mass fluxes. For this problem we examine the dry mass budget, which is the simplest case because there is no source term in (6). Various previous studies have investigated hemispheric mass (e.g. Trenberth 1981) and Zhao and Li (2006) found large discrepancies in the cross equatorial mass flux from several reanalyses including ERA-40. Here, we concentrate almost exclusively on the hemispheric dry mass budget.

The tendency of the area average dry mass, mda, is given by the average over an area A of (6) so that

$$\frac{\partial m_{da}}{\partial t} = -\frac{1}{A}\int dA\underline{\nabla}\cdot\frac{1}{g}\int_0^1 \underline{v}(1-q)\frac{\partial p}{\partial \eta}d\eta = \frac{1}{A}\oint dl\,\frac{1}{g}\int_0^1 v(1-q)\frac{\partial p}{\partial \eta}d\eta \qquad (7)$$

where v is the inward pointing wind normal to the line l around the area. This relation links the tendency of m_{da} to the area averaged convergence of vertically integrated dry mass fluxes, C, which is related by Gauss's Theorem to the line averaged vertically integrated dry mass flux, V, into the area. In other words,

$$\frac{\partial m_{da}}{\partial t} = C = V\frac{l}{A} \tag{8}$$

where C is measured in $kgm^{-2}s^{-1}$ and V in $kgm^{-1}s^{-1}$. In the case of a hemisphere, the average cross equatorial mass flux, $V = Ca$, where a is the radius of the earth.

Figure 4a shows the monthly mean time series of dry mass for ERA-Interim in the two hemispheres to be highly anti-correlated. On average, the mass in the Southern Hemisphere is smallest in February with 10040.1 kgm^{-2} (Table 4) while in the Northern Hemisphere it is largest in February with 10010.5 kgm^{-2}. The difference of 29.6 kgm^{-2}, which is at a minimum, rises to a maximum value of 81.1 kgm^{-2} during July.

The tendencies of the NH area average dry mass in ERA-Interim and ERA-40 are in good agreement (Figure 4b) and are an order of magnitude larger than the global tendencies (Figure 3c). This is an indication that the analysed global dry mass is well conserved in comparison with variations on the hemispheric scale.

For ERA-Interim, the hemispheric dry mass tendencies of the average annual cycle in both hemispheres show that dry mass flow into the Southern Hemisphere is maximised in May while flow into the NH is maximised in September, with peak magnitudes of about 0.3 $kgm^{-2}day^{-1}$ (Table 4) or 1.91 $Ggm^{-1}day^{-1}$.

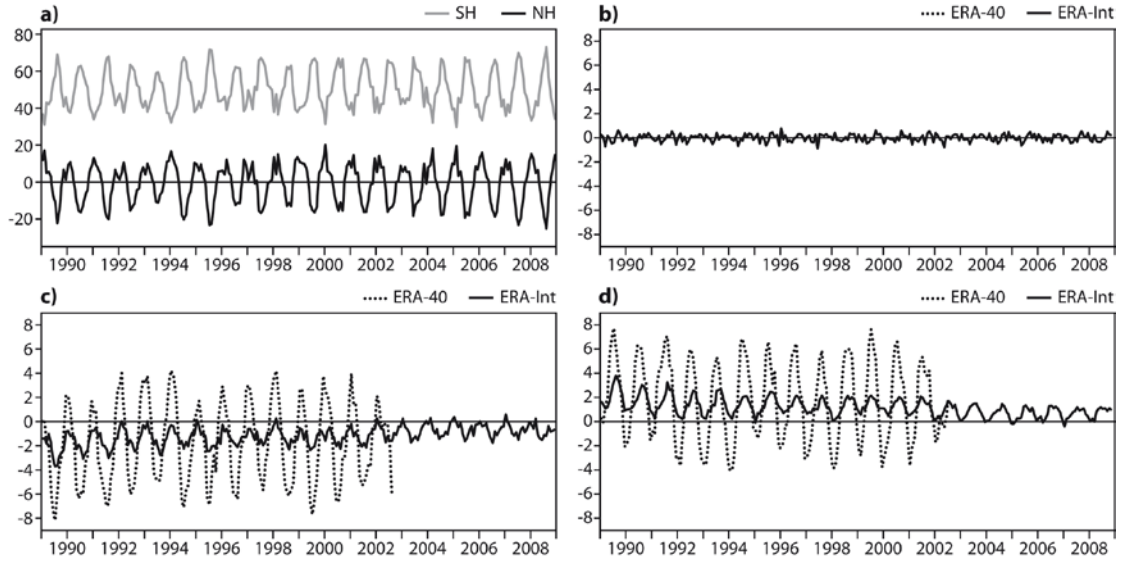

Figure 4: Vertically integrated monthly mean time series from 1989 to 2008 of a) NH (solid) and SH (grey) dry mass in ERA-Interim, b) NH dry mass tendency, c) NH convergence of dry mass fluxes and d) NH dry mass budget residual (tendency-convergence). The curves in b), c) and d) are for ERA-Interim (solid) and ERA-40 (dashed). The units in a) are kgm^{-2} - 10000, and in b), c) and d) they are $kgm^{-2}day^{-1}$.

	SH dry mass	NH dry mass	SH dry mass tendency	NH dry mass tendency	NH dry mass convergence	ERA-40 NH dry mass convergence
Jan	40.3	10.1	-0.11	+0.11	-0.32	+2.50
Feb	40.1	10.5	-0.02	+0.02	-0.45	+2.33
Mar	41.4	9.0	+0.16	-0.17	-0.77	+0.62
Apr	45.6	4.5	+0.07	-0.08	-0.92	-0.86
May	51.4	-1.8	+0.32	-0.34	-1.49	-3.80
Jun	61.8	-12.5	+0.25	-0.25	-1.75	-5.92
Jul	65.3	-15.8	+0.02	-0.01	-1.87	-6.28
Aug	65.1	-15.6	-0.05	+0.06	-1.97	-5.63
Sep	59.6	-9.8	-0.32	+0.32	-1.52	-3.70
Oct	50.8	-0.8	-0.22	+0.23	-1.37	-2.75
Nov	43.7	6.5	-0.22	+0.22	-0.93	-0.22
Dec	41.5	8.6	+0.09	-0.10	-0.71	+1.88
Ann	50.6	-0.6	0.00	0.00	-1.18	-1.84
Max-Min	25.2	26.3	0.64	0.66	1.65	8.78

Table 4: Annual cycle of NH and SH dry mass and dry mass tendencies and the convergence of dry mass fluxes into the NH. For dry mass the units are kgm^{-2} -10000, otherwise they are kgm^{-2}day^{-1}. All columns are for ERA-Interim (1989-2008) except the last column which is for ERA-40 (1989-2001).

The NH averaged convergence of vertically integrated dry mass fluxes, C, in ERA-Interim does not agree well with the hemispheric tendencies on monthly time scales (Figure 4) or for the mean annual cycle (Table 4). The convergence is so negatively biased (indicating that the flow is directed preferentially into the Southern Hemisphere) that the mean annual cycle shows negative values for all months of the year with a large peak magnitude of 2.0 kgm^{-2}day^{-1}, which is more than six times larger than that of the hemispheric mass tendencies. As discussed above, the mass is thought to be reasonably well analysed, so it would appear that it is the convergence that is poorly captured by the analysis. Interestingly, the NH convergence does appear to improve with time. The peak magnitude of nearly 4 kgm^{-2}day^{-1} occurs during 1989 but by 2002 this has decreased to less than 2 kgm^{-2}day^{-1}. While the convergence in ERA-40 does indicate more northward flow, the magnitudes are an order of magnitude too large, with a peak value of -6.3 kgm^{-2}day^{-1} in the average annual cycle (Figure 4b and Table 4). Curiously, unlike in ERA-Interim, the convergence in ERA-40 does not appear to improve with time. The NH budget residual (tendency-convergence) is a measure of the degree to which the tendency of the analysed mass agrees with the analysed convergence of mass fluxes into the NH (Figure 4d). It is clear that the agreement is not good and the residual is dominated by the convergence term.

These results are for dry mass, so it could be possible that the cross equatorial flux of *TCWV* is responsible for the poor and varying quality of this cross equatorial dry mass flux. However, the cross equatorial flux of *TCWV* has a relatively small magnitude and is stable, both in time and between ERA-Interim and ERA-40, so the same qualitative picture emerges from studying the cross equatorial total mass flux (not shown), though in that case the *E-P* must also be taken into account.

The dry mass budget residual for six regions of the globe is shown in Figure 5. They all have the common feature that the residual is much better in ERA-Interim than in ERA-40. The two regions where the residual is worst, i.e. largest, are the two polar caps, 90°N-60°N and 60°S-90°S. The two regions, 90°N-30°N and 30°S-90°S, are intriguing because in contrast to the hemispheric results, the ERA-Interim residuals are small during 1989-2002 and become larger thereafter.

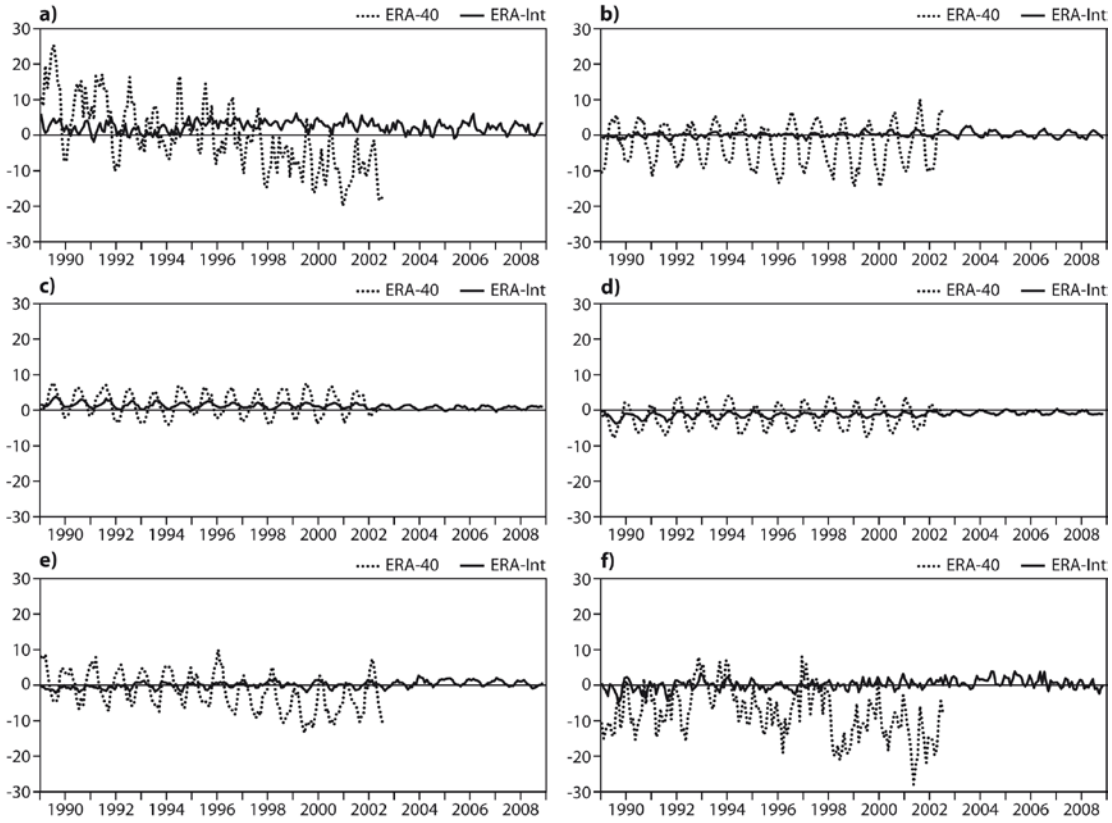

Figure 5: Vertically integrated monthly mean time series from 1989 to 2008 for ERA-Interim (solid) and ERA-40 (dashed) of dry mass budget residual (tendency-convergence) for a) 90°N-60°N, b) 90°N-30°N, c) NH, d) SH, e) 30°S-90°S and f) 60°S-90°S. The units are $kgm^{-2}day^{-1}$.

3.3 Time averaged mass and moisture budgets

Now we look at the time averaged budgets of mass and moisture, where the tendency term is considered to be zero and the divergence term should balance the source term, if any.

In ERA-Interim for 1989-2008 the divergence of the moisture fluxes are well balanced locally by *E-P* (Figure 6a and 6b). The residual (divergence-(*E-P*)) (Figure 6d) is generally smaller than the individual terms. The global average of the residual (which is the global average of *P-E* because the global average divergence is zero) is 0.003 $kgm^{-2}day^{-1}$ and the global standard deviation is 0.3 $kgm^{-2}day^{-1}$. Note that as previously discussed, the global mean does vary depending on the period considered, see Figure 3d. In ERA-40 the balance is poorer, particularly over the tropical oceans where the residuals are larger than 2 $kgm^{-2}day^{-1}$ over large areas, again reflecting the poor representation of the hydrological cycle. The global average of the residual (for 1989-2001) is 0.5 $kgm^{-2}day^{-1}$ and the standard deviation is 1.1 $kgm^{-2}day^{-1}$.

In the time average, the divergence of dry mass fluxes is equivalent to the budget residual because there is no source term in (6). The dry mass divergence is generally smaller in ERA-Interim than in ERA-40 (Figures 6c and 7c), where the global standard deviation is 10 and 25 $kgm^{-2}day^{-1}$ for the two reanalyses respectively. However, these values are large compared with those for the moisture budget residuals, see above, and *E-P* (Figures 6b and 7b), where the global standard deviations are 2.1 and 2.8 $kgm^{-2}day^{-1}$ respectively. Although it is not necessary to mass adjust the divergence of the moisture fluxes, the large values of dry mass divergence seen in this and the previous sub-section indicate that in some cases it will be necessary to mass adjust the divergence of fluxes, even in ERA-Interim, as done for example by Trenberth (1991) and Chiodo and Haimberger (2010).

The net effect of the hydrological cycle in the atmosphere is to evaporate water from the oceans and transport it to land where it is rained out. We now use this idea to give us a simple physical measure of how well the moisture divergence and *E-P* fields match in Figures 6a and b and 7a and b. Each of these three processes should involve the same amount of water. So, the integral of *E-P* over ocean should equal the atmospheric transport of *TCWV* from ocean to land (the integral of moisture divergence over ocean) which, in turn, should equal the integral of *P-E* over land. In ERA-Interim for 1989-2008 the transport of 1.1 Tgs^{-1} is weaker than the oceanic *E-P* and land *P-E* of 1.2 Tgs^{-1}, though the oceanic *E-P* is smaller for the 1989-2001 period (Table 5). The magnitudes for *E-P*, *P-E* and transport are larger for ERA-40 and the oceanic *E-P* has the wrong sign due to the unrealistically large values of tropical precipitation (Uppala 2005).

	Ocean E-P	***TCWV* Transport**	**Land P-E**
EI 20	1.22	1.06	1.24
EI 13	1.05	1.00	1.21
E4 13	-1.39	1.22	1.35

Table 5: E-P over ocean (defined to be positive into the atmosphere), the atmospheric transport of TCWV from the oceans to land and P-E over land (defined to be positive out of the atmosphere) in ERA-Interim (EI) and ERA-40 (E4) for the 20 year period 1989-2008 and 13 year period 1989-2001. The units are Tgs^{-1}.

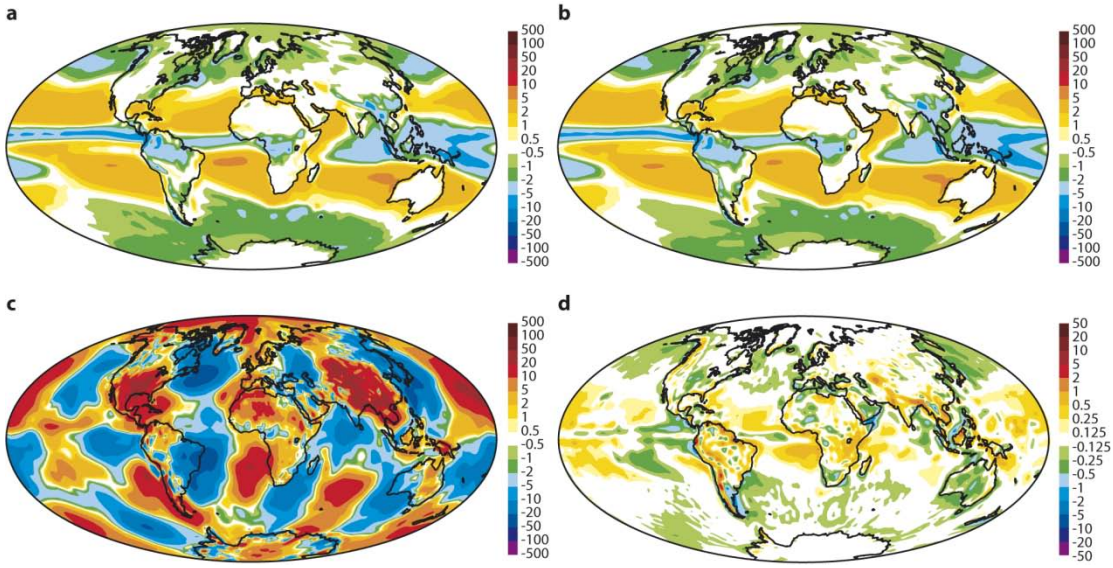

Figure 6: Time averaged vertically integrated mass and moisture budgets for ERA-Interim for 1989-2008 showing a) divergence of moisture fluxes, b) E-P (defined to be positive upwards into the atmosphere), c) divergence of dry mass fluxes and d) moisture budget residual (divergence – (E-P)). The units are $kgm^{-2}day^{-1}$. All fields shown have been smoothed using a Hoskins spectral filter with an attenuation of 0.1 at wavenumber 106.

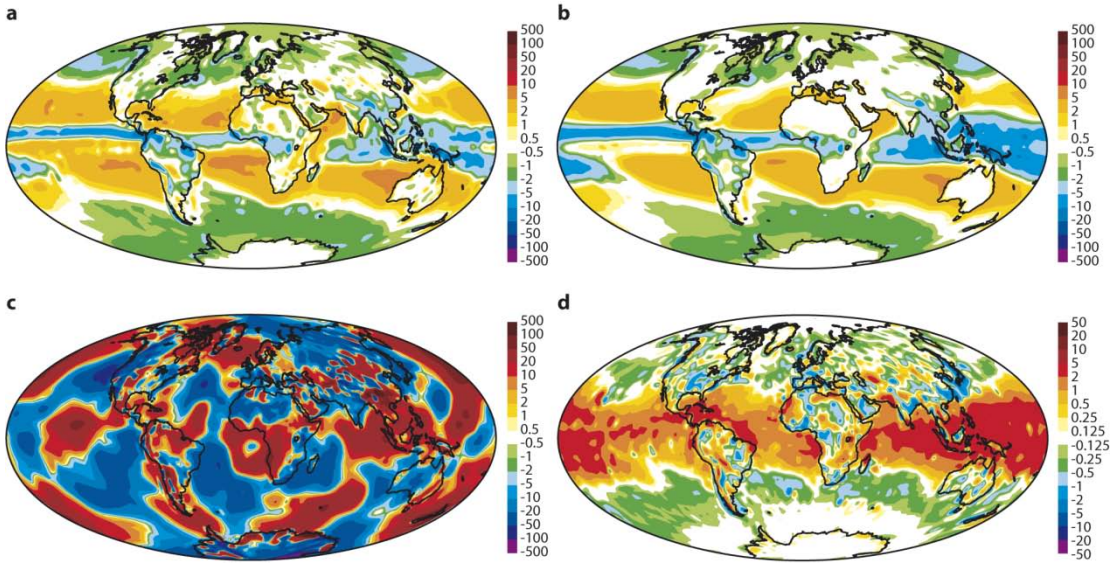

Figure 7: As Figure 6 but for ERA-40 for 1989-2001.

4 Energy

Global energy is another fundamental property of the atmosphere which has a particular significance today because of the need to monitor the planet for signs of global warming. Trenberth *et al.* (2009) (hereafter TFK09) examined the global energy flows in the atmosphere for the period March 2000 to May 2004 using a mixture of observations, reanalyses and theory. Here, we investigate the top of the atmosphere (TOA) incident solar radiation, the energy balances at the TOA and at the surface (Figure 8) and then investigate the budget of total atmospheric energy.

4.1 Top of atmosphere incident solar radiation

The TOA incident solar radiation (TSRD) from various reanalyses is shown in Table 6. Note that the values for ERA-40 are not archived, so have been estimated. It is clear that the global values in ERA-Interim and ERA-40 are larger than the more usual value of 341.3 Wm^{-2} by about 3 and 2 Wm^{-2} respectively. The main reason for this error is that there is a bug in the solar radiation scheme of the ERA forecast system used to produce both sets of ERA products, which results in an increase of about 2 Wm^{-2} in TSRD. This bug has since been corrected for operational and future use, but not for ERA-Interim. In the latter, there is a further increase of about 1 Wm^{-2} in TSRD due to setting the solar constant at 1370 Wm^{-2} instead of 1366 Wm^{-2}, as in ERA-40. In addition, TSRD in ERA-Interim has no specified 11-year solar cycle.

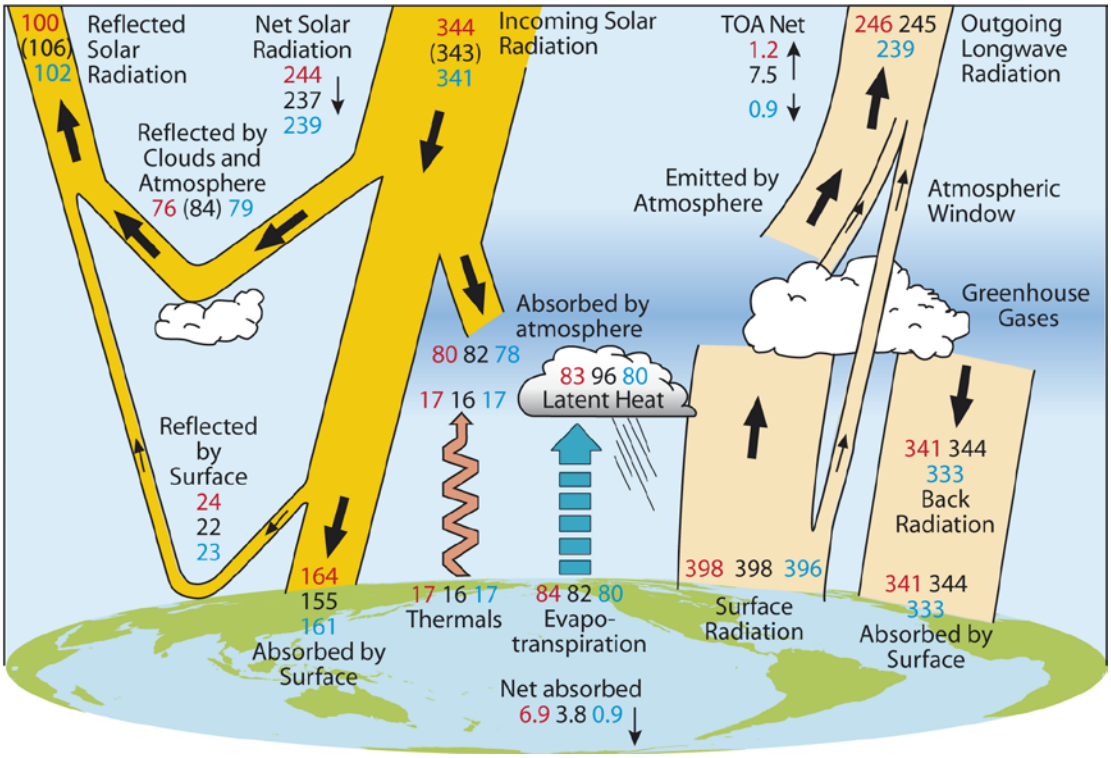

*Figure 8: Global atmospheric energy flows (Wm^{-2}) in ERA-Interim (red) for 1989-2008, ERA-40 (black) for 1989-2001 and TFK09 (blue) for March 2000-May 2004. The ERA-40 values in parentheses are estimated. Image adapted from Trenberth, K.E., J.T. Fasullo and J. Kiehl, 2009: Earth's global energy budget. Bull. Amer. Meteor. Soc., **90**, No. 3, 311-324, doi:10.1175/2008BAMS2634.1 ©American Meteorological Society. Reprinted with permission.*

	Dataset	Globe	Oceans	Land
TOA solar	ERA-Interim	344.2	350.2	329.2
radiation	ERA-40	(343)	(349)	(328)
downward	JRA-25	341.3	347.6	326.0
(TSRD)	NRA2	341.3	347.0	327.0
	TFK09	341.3	345.4	330.2
TOA net solar	ERA-Interim	244.3	254.7	218.6
radiation	ERA-40	237.2	244.8	218.6
(TSRN)	JRA-25	246.8	256.6	223.5
	NRA2	236.2	243.3	218.3
	TFK09	239.4	247.7	216.8
TOA net	ERA-Interim	-245.5	-248.2	-239.0
thermal	ERA-40	-244.7	-246.9	-239.2
radiation	JRA-25	-254.6	-256.9	-249.1
(OLR)	NRA2	-243.3	-245.7	-237.2
	TFK09	-238.5	-240.8	-232.4
TOA net	ERA-Interim	-1.2	+6.5	-20.3
energy	ERA-40	-7.5	-2.1	-20.6
(R_T)	JRA-25	-7.8	-0.3	-25.6
	NRA2	-7.1	-2.4	-18.9
	TFK09	+0.9	+6.9	-15.6

Table 6: Top of atmosphere (TOA) energy budget over the globe, oceans and land for ERA-Interim (1989-2008), ERA-40 (1989-2001), JRA (1989-2008), NRA2 (1989-2008) and TFK09 (March 2000-May 2004). The units are Wm^{-2} and fluxes are defined to be positive downwards. The ERA-40 values in parentheses are estimated values.

4.2 Top of atmosphere energy balance

The agreement in the global TOA net thermal radiation (OLR) between ERA-Interim, with a value of 246 Wm^{-2}, and ERA-40 is to within 1 Wm^{-2} but is 7 Wm^{-2} larger than the estimate given by TFK09 (Table 6 and Figure 8). The global TOA net solar radiation (TSRN) of 244 Wm^{-2} in ERA-Interim is 7 Wm^{-2} larger than in ERA-40, with the difference originating in the larger reflection of solar radiation over oceanic regions in ERA-40, and 5 Wm^{-2} larger than in TFK09. The resulting TOA input of energy to the atmosphere, R_T, for the globe is quite small in ERA-Interim, with a value of -1.2 Wm^{-2} (a loss of energy), as compared to -7.5 Wm^{-2} in ERA-40 and -7 Wm^{-2} in both NRA2 and JRA-25. Unfortunately, the small energy loss at the top of the atmosphere in ERA-Interim is subject to spin-up and increases by about 25% during the subsequent 12 hours of the forecasts from 12 to 24 hours. The TOA energy losses in these reanalyses should be contrasted with the TOA energy gain of 0.9 Wm^{-2} specified by TFK09 in order to account for the current warming of our planet.

We now estimate the temporally averaged spatial errors of R_T in ERA-Interim by comparing the latter (adjusted to have zero global mean) with adjusted CERES data, which are thought to be accurate to within a few Wm^{-2} (Fasullo and Trenberth 2008a). The CERES TOA 2001-2009 annual climatology of radiative fluxes were adjusted so that the global average of R_T would be 0.9 Wm^{-2}. This was achieved by increasing the magnitude of OLR by 1.5 Wm^{-2} everywhere and uniformly increasing the albedo from 0.284 to 0.290. This adjustment is similar to that done by Fasullo and Trenberth (2008a), which was used by TFK09. In general, the errors in R_T for ERA-Interim are negative in the tropics, where the deficit reaches more than 50 Wm^{-2} over South America. Over the Southern Ocean R_T in ERA-Interim is more than 10 Wm^{-2} too large over large areas (Figure 9) and it is also too large over much of the extratropical Northern Hemisphere. These errors indicate that the meridional gradient of R_T is too small in ERA-Interim, with too little radiation being absorbed at low latitudes and not enough being lost at high latitudes. These errors are qualitatively similar to those found for JRA-25 by Trenberth and Fasullo (2010) and for ERA-40 by Trenberth and Smith (2009) and which were found to be due to clouds over the tropical oceans having too large an albedo while there was too little cloud over low latitude land and over the higher latitudes, particularly over the Southern Ocean (Trenberth and Fasullo 2010).

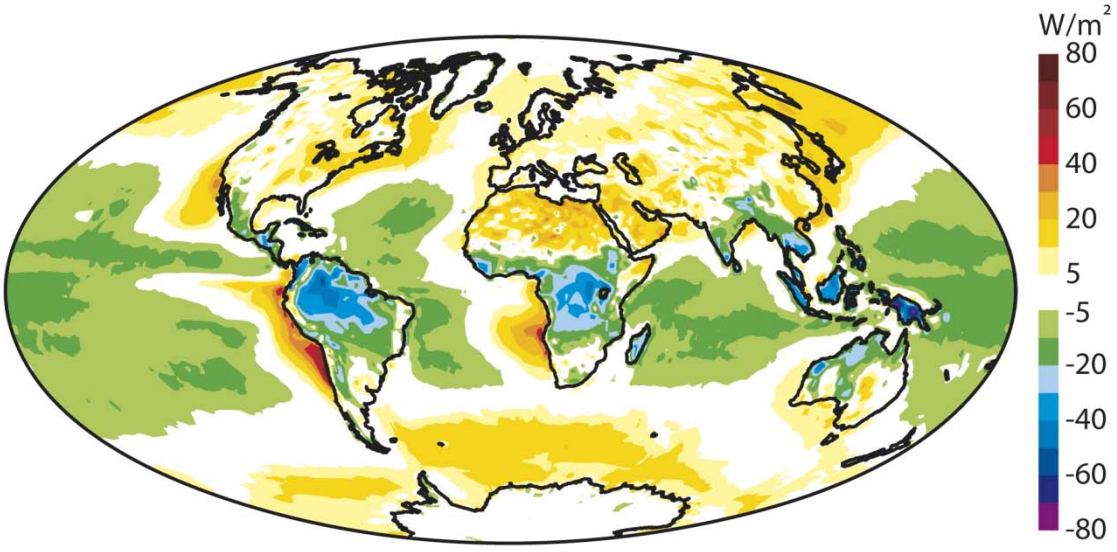

Figure 9: TOA adjusted energy input (R_T) for ERA-Interim minus CERES data for the years 2001-2009. The units are Wm^{-2}.

4.3 Surface energy balance

At the surface the global downwelling thermal radiation (STRD) in ERA-Interim is 341 Wm^{-2}, which is about 3 Wm^{-2} less than in ERA-40 (Figure 8) but 8 Wm^{-2} larger than in TFK09, with the bulk of this latter discrepancy originating over the oceans (Table 7a). The values for JRA-25 are 15 Wm^{-2} smaller than in ERA-Interim, being only 326 Wm^{-2}. The value of 398 Wm^{-2} in ERA-Interim for the surface global upwelling thermal radiation (STRU) agrees to within 2 Wm^{-2} with the values from ERA-40, TFK09, NRA2 and JRA-25. The downward solar radiation at the surface (SSRD) is 188 Wm^{-2} in ERA-Interim, which is 10 and 4 Wm^{-2} larger than those in ERA-40 and TFK09 respectively. The

values for JRA-25 are 9 Wm^{-2} larger than for ERA-Interim. The global values of the surface turbulent fluxes of sensible heat (SSHF) for ERA-Interim are 17 Wm^{-2} and agree to within about 2 Wm^{-2} with ERA-40 and TFK09 (Table 7b). However, the SSHF for NRA2 is less than half that of the other estimates. The global value of the surface turbulent fluxes of latent heat (SLHF) for ERA-Interim is 84 Wm^{-2} which agrees with ERA-40 to within 1 Wm^{-2} but is 4 Wm^{-2} greater than in TFK09 while the values from JRA-25 and NRA2 are 6 and 9 Wm^{-2} more intense respectively.

	Dataset	Globe	Oceans	Land
Sfc solar	ERA-Interim	188.1	188.4	187.2
radiation	ERA-40	177.7	178.1	176.6
downward	JRA-25	196.8	193.7	204.3
(SSRD)	NRA2	187.3	185.3	192.5
	TFK09	184.3	184.4	184.7
Sfc solar	ERA-Interim	-23.8	-14.2	-47.5
radiation	ERA-40	-22.3	-13.8	-43.4
upward	JRA-25	-25.1	-13.4	-53.0
(SSRU)	NRA2	-26.9	-17.9	-49.5
	TFK09	-23.1	-16.6	-39.6
Sfc thermal	ERA-Interim	341.2	356.2	303.9
radiation	ERA-40	344.2	359.4	306.3
downward	JRA-25	326.1	342.2	287.5
(STRD)	NRA2	340.0	356.7	298.1
	TFK09	333.0	343.3	303.6
Sfc thermal	ERA-Interim	-397.7	-408.6	-370.6
radiation	ERA-40	-397.7	-408.5	-371.0
upward	JRA-25	-398.7	-409.7	-372.4
(STRU)	NRA2	-396.9	-407.9	-369.1
	TFK09	-396.0	-400.7	-383.2

Table 7a. Upward and downward radiative fluxes for the surface energy budget over the globe, oceans and land for ERA-Interim (1989-2008), ERA-40 (1989-2001), JRA (1989-2008), NRA2 (1989-2008) and TFK09 (March 2000-May 2004). The units are Wm^{-2} and fluxes are defined to be positive downwards.

	Dataset	Globe	Oceans	Land
Sfc net solar	ERA-Interim	164.3	174.2	139.7
radiation	ERA-40	155.4	164.3	133.2
(SSRN)	JRA-25	171.8	180.3	151.3
	NRA2	160.5	167.4	143.0
	TFK09	161.2	167.8	145.1
Sfc net	ERA-Interim	-56.5	-52.4	-66.7
thermal	ERA-40	-53.5	-49.0	-64.7
radiation	JRA-25	-72.6	-67.6	-84.8
(STRN)	NRA2	-56.9	-51.2	-71.1
	TFK09	-63.0	-57.4	-79.6
Sfc sensible	ERA-Interim	-17.4	-13.1	-28.2
heat flux	ERA-40	-15.7	-11.5	-26.0
(SSHF)	JRA-25	-19.3	-16.3	-26.6
	NRA2	-7.8	-5.9	-12.4
	TFK09	-17.0	-12.0	-27.0
Sfc latent	ERA-Interim	-83.5	-99.3	-44.3
heat flux	ERA-40	-82.4	-99.0	-41.2
(SLHF)	JRA-25	-89.3	-110.7	-38.1
	NRA2	-92.2	-108.0	-52.6
	TFK09	-80.0	-97.1	-38.5
Sfc net	ERA-Interim	6.9	9.4	0.5
energy	ERA-40	3.8	4.7	1.3
(F_S)	JRA-25	-9.5	-14.2	1.7
	NRA2	3.6	2.3	7.0
	TFK09	0.9	1.3	0.0

Table 7b. Net fluxes for the surface energy budget over the globe, oceans and land for ERA-Interim (1989-2008), ERA-40 (1989-2001), JRA (1989-2008), NRA2 (1989-2008) and TFK09 (March 2000-May 2004). The units are Wm^{-2} and fluxes are defined to be positive downwards.

In ERA-Interim, compared with ERA-40, some of the excess of downward solar radiation over land is reflected away and the remaining terms in the surface energy budget appear to more than compensate for the increase in solar radiation to give a net land surface energy imbalance of only 0.5 Wm^{-2} which is an improvement of 0.8 Wm^{-2} over ERA-40. Over the oceans, however, the compensation is not so large and the net surface energy imbalance is larger in ERA-Interim than in ERA-40. The global net loss of energy to the surface, F_S, is 6.9 and 3.8 Wm^{-2} in ERA-Interim and ERA-40 respectively (Figure 8 and Table 7b). The values of F_S in JRA-25 and NRA2 are -9.5 (a gain of energy for the atmosphere) and 3.6 Wm^{-2} while in TFK09 it is specified to be 0.9 Wm^{-2}, which is required to satisfy current estimates of ocean warming. These reanalysis surface energy losses are quite considerable and the loss

of 6.9 Wm^{-2}, for example, would lead to a loss of about 4355 MJm^{-2} over twenty years, which is greater than the total energy of the atmosphere (2623 MJm^{-2}). There is some improvement of F_S in ERA-Interim due to spin-down, where the surface energy imbalance decreases on average by about 13% during the subsequent 12 hours of the forecast from 12 to 24 hours.

4.4 Total energy of the atmosphere

Following, for example, Boer (1982) and Trenberth and Solomon (1994) the total energy in an atmospheric column, *TE*, is given by

$$TE = \frac{1}{g}\int_0^1 (Lq + C_p T + \Phi_S + k)\frac{\partial p}{\partial \eta} d\eta \tag{9}$$

where L, C_p, T, Φ_s and k are the latent heat of condensation of water, the specific heat capacity of air at constant pressure, which depends on q (Källberg *et al.* 2004), temperature, surface geopotential and kinetic energy ($(\underline{v}\cdot\underline{v})/2$) respectively. The evolution of *TE* is determined from

$$\frac{\partial TE}{\partial t} = -\underline{\nabla}\cdot\frac{1}{g}\int_0^1 \underline{v}(h+k)\frac{\partial p}{\partial \eta} d\eta + TEI \tag{10}$$

where $h = Lq + C_p T + \Phi$ is the moist static energy (Φ is geopotential), and $TEI = R_T - F_S$ is the input of energy to the atmosphere by the net fluxes of energy at the TOA and surface, which were discussed above. The effects of frictional dissipation are small and have been neglected (Trenberth and Solomon 1994).

The global integral of the convergence term on the rhs of (10) is zero, so that the evolution of the *TE* of the global atmosphere is governed simply by *TEI*. The absence of any divergent flux in the global case means that we do not have to worry about spurious divergent mass fluxes.

The mean annual cycle for the analysed global *TE*, whose peak to peak range is about 1% of the annual climate value of 2623 MJm^{-2}, reaches a maximum in July and a minimum in either December or January (Table 8). The agreement in TE between ERA-Interim and ERA-40 is good but the annual climate for the latter is 0.1% larger than for the former. The monthly mean anomalies of *TE* for the two ERA datasets also show a good correspondance (Figure 10a) and are quite stable with no large trends. The standard deviation of the anomalies and linear trends for TE in ERA-Interim for the period 1989-2008 are 3 MJm^{-2} and 1 $MJm^{-2}decade^{-1}$ while in ERA-40 for the period 1989-2001 they are 3 MJm^{-2} and 3 $MJm^{-2}decade^{-1}$ respectively. These values are small compared to the global *TE* of the atmosphere. The most notable event in this time series is the temporary increase in *TE* by about 9 MJm^{-2} which lagged by several months the increase in the Nino3.4 SST index associated with the 1997-1998 El Niño. There are also shifts of about 3 MJm^{-2}, to lower values in 1992 and back to higher values from 2001, which are consistent with the shifts of 1 kgm^{-2} in TCWV discussed in Section 3.1.

	EI 20	EI 13	E4 13
Jan	2613.6	2612.3	2614.9
Feb	2615.6	2614.7	2616.8
Mar	2617.6	2616.8	2618.9
Apr	2621.2	2620.5	2623.1
May	2626.4	2626.1	2629.0
Jun	2633.2	2632.7	2635.5
Jul	2638.0	2637.4	2640.1
Aug	2636.4	2635.8	2638.8
Sep	2628.3	2627.3	2630.0
Oct	2619.8	2618.8	2621.2
Nov	2614.2	2613.5	2616.0
Dec	2613.1	2612.5	2615.3
Ann	2623.2	2622.4	2625.0
Max-min	24.9	25.1	25.2

Table 8: Mean annual cycle of total energy (TE) in ERA-Interim (EI) and ERA-40 (E4) for the 20 year period 1989-2008 and 13 year period 1989-2001. The units are MJm^{-2}.

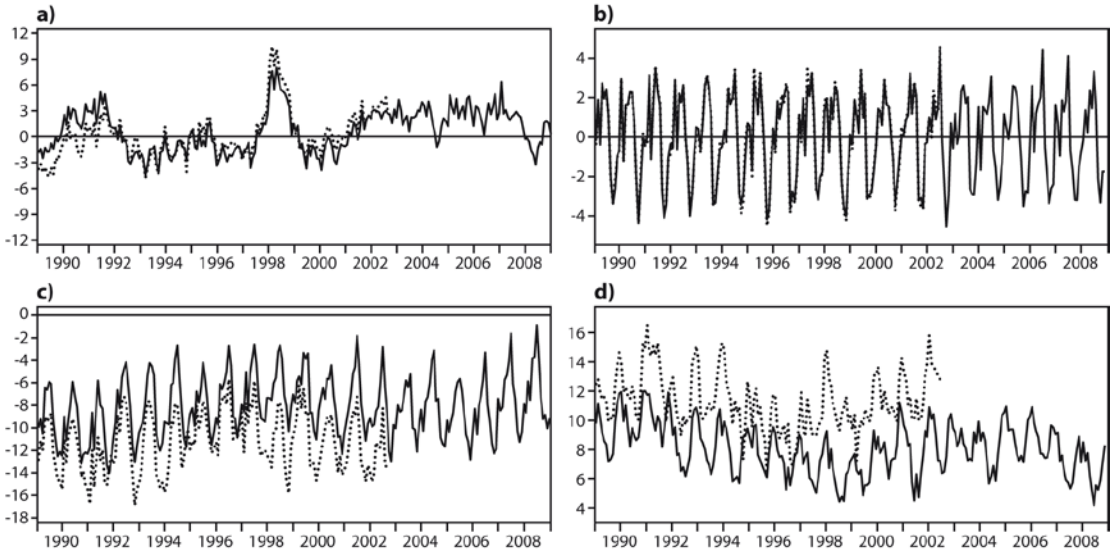

Figure 10: Vertically integrated global monthly mean time series from 1989 to 2008 for ERA-Interim (solid) and ERA-40 (dashed) of a) analysed total atmospheric energy (TE) anomaly, b) total energy tendency, c) energy input (TEI) and d) energy budget residual (energy tendency-energy input). The units in a) are MJm^{-2} and in b), c) and d) they are Wm^{-2}. The reference period in a) is 1989-2001.

A consequence of a stable TE with a small standard deviation and trend is that, on average, the energy tendencies are close to zero in ERA-Interim and ERA-40 (Figure 10b). However, the combined effect of *RT* and F_S give rise to a net loss of energy that is far from zero (Figure 10c), with average values of 8 and 11 Wm^{-2} in ERA-Interim and ERA-40 respectively. The energy budget residual (*TE* tendency - *TEI*), which is equal to the monthly average of the analysis increments for energy divided by the length of the forecast (12 hours), is not close to zero, though it is smaller in ERA-Interim than in ERA-40 (Figure 10d). The energy increments in ERA-Interim vary on long timescales, as also found by Chiodo and Haimberger (2010), but the variation is not straightforward. The values decrease from 1989 to 1999, then increase to 2005 and then decrease again to 2008.

Now we look spatially at the time averaged budgets of *TE* where the tendency term in (10) is considered to be zero and the divergence term should balance the energy input, *TEI*. In ERA-Interim for 1989-2008 the divergence of the mass adjusted (following Chiodo and Haimberger 2010) energy fluxes is reasonably well balanced locally by *TEI* (Figures 11a and 11b) and the residual (adjusted divergence - *TEI*) (Figure 11d) is generally smaller than the individual terms. The global average of the residual is 8 Wm^{-2} and the global standard deviation is 11 Wm^{-2}. In ERA-40 for 1989-2001 the balance is much poorer over much of the globe (Figure 12) with the average of the residual being 11 Wm^{-2} and the standard deviation 25 Wm^{-2}.

In ERA-Interim the balance between the *TE* divergence and *TEI* is worse if the divergence of the energy fluxes is not mass adjusted (compare Figure 11c with 11a and b) and for ERA-40 the balance is much worse (Figure 12). The global standard deviation of the residual using the unadjusted divergence is 38 and 95 Wm^{-2} in ERA-Interim and ERA-40 respectively. Even though the problem is not as accute in ERA-Interim as in ERA-40, it is still necessary to mass adjust energy fluxes and their divergence in both reanalyses.

The net effect of the energy cycle of the atmosphere is that energy is absorbed at the TOA at low latitudes, some of which is lost to the surface while the remainder is transported to high latitudes which then, augmented by energy from the surface, is lost to space. A schematic diagram of these processes is shown in Figure 13. We now use this idea to give us a simple physical measure of how well the *TE* divergence and *TEI* fields match in Figures 11a and 11b and Figures 12a and 12b. The difference between the energy in at the TOA and out at the surface at low latitudes (the spatial integral of *TEI*) should match the energy transport from low to high latitudes (the integral of *TE* divergence over low latitudes) which, in turn, should match the difference between the energy out at the TOA and in at the surface at high latitudes (the spatial integral of -*TEI*). The low latitudes are defined as 40°N-40°S with the remainder of the globe defined as the high latitudes. The region 40°N-40°S was chosen because its boundaries approximately coincide with the latitudes of zero *TEI* and energy divergence and the largest poleward energy fluxes, see Trenberth and Carron (2001) and Fasullo and Trenberth (2008b).

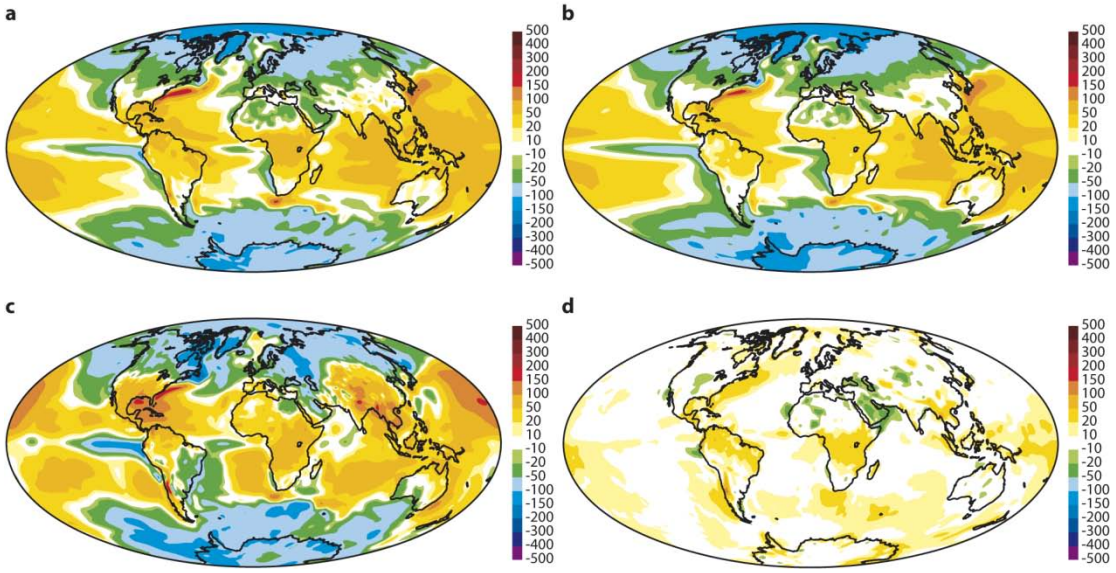

Figure 11: Time averaged vertically integrated total energy (TE) budget for ERA-Interim for 1989-2008 showing a) mass adjusted divergence of energy fluxes, b) energy input (TEI), c) unadjusted divergence of energy fluxes and d) energy budget residual (adjusted divergence – energy input). The units are Wm^{-2}. All fields shown have been smoothed using a Hoskins spectral filter with an attenuation of 0.1 at wavenumber 106.

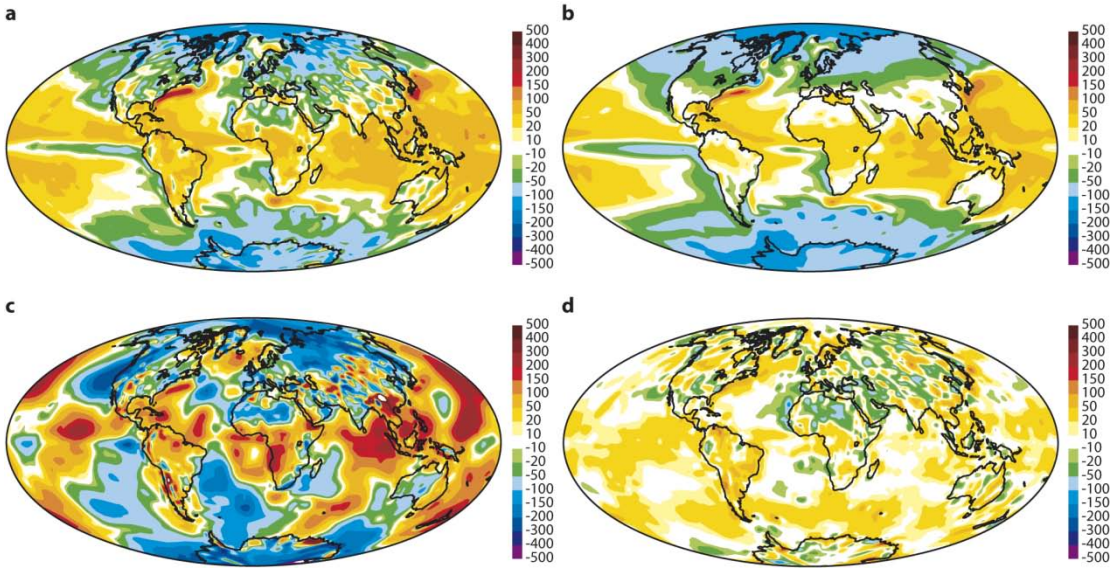

Figure 12: As Figure 11 but for ERA-40 for 1989-2001.

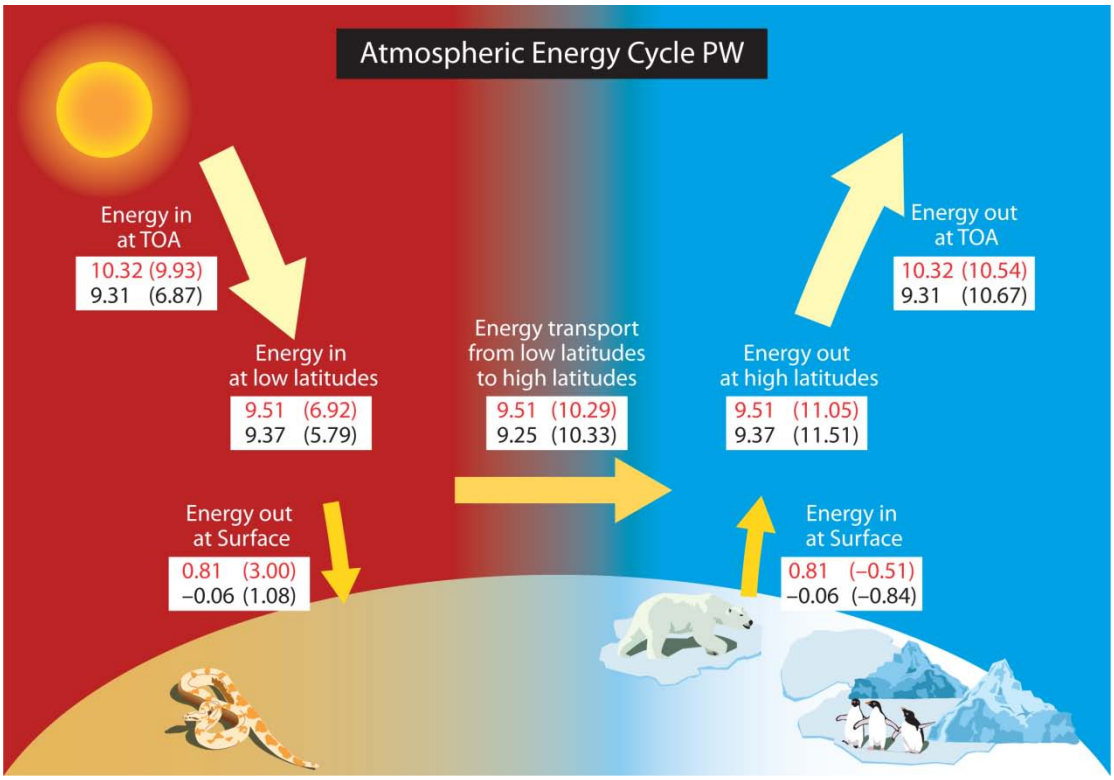

Figure 13: Atmospheric energy cycle. Energy is absorbed at the TOA at low latitudes, some of which is lost to the surface while the remainder is transported to high latitudes and then, augmented by energy from the surface, is lost to space. Each of these processes is depicted by an arrow with the adjusted values (PW) for ERA-Interim for 1989-2008 (red) and ERA-40 for 1989-2001 (black). The difference between the energy in at the TOA and out at the surface at low latitudes (left hand middle box) should match the energy transport from low to high latitudes which, in turn, should match the difference between the energy out at the TOA and in at the surface at high latitudes (right hand middle box). The low latitudes are defined as 40°N-40°S with the remainder of the globe defined as the high latitudes. The unadjusted values are shown in parentheses.

	Low lat TEI	TE Transport	High lat -TEI
EI 20	9.51 (6.92)	9.51 (10.29)	9.51 (11.05)
EI 13	9.33 (6.73)	9.48 (10.32)	9.33 (10.86)
E4 13	9.37 (5.79)	9.25 (10.33)	9.37 (11.51)

Table 9: The adjusted energy input to the atmosphere (TEI) over low latitudes, the mass adjusted atmospheric transport of total energy (TE) from low to high latitudes and the adjusted energy loss from the atmosphere (–TEI) over the high latitudes in ERA-Interim (EI) and ERA-40 (E4) for the 20 year period 1989-2008 and 13 year period 1989-2001. The low latitudes are defined to be 40°N-40°S while the remainder of the globe defines the high latitudes. The unadjusted values are shown in parentheses. The units are PW.

The mass adjusted horizontal atmospheric energy transports of 9.5 and 9.3 PW (the unadjusted transports are 10.3PW) for ERA-Interim and ERA-40 respectively (Table 9 and Figure 13) are similar to the sum of the peak atmospheric energy transports from the two hemispheres (about 5 PW in each) given by Trenberth and Carron (2001) and Fasullo and Trenberth (2008b). However, the horizontal transports are weaker than the energy losses at high latitudes, which range from 10.9 PW for ERA-Interim in the period 1989-2001 to 11.5 PW for ERA-40 in the same period (Table 9). A large part of this mismatch at high latitudes originates in the SH. The energy inputs at low latitudes are much weaker than the transports, varying from 6.9 PW for ERA-Interim in the period 1989-2008 to 5.8 PW for ERA-40. The mismatches between the three processes can be reduced by making simple global adjustments to *TEI*. If the annual climate of R_T is adjusted to have zero global mean and F_S is set to zero over land and adjusted to have zero mean over ocean, then the energy inputs at low latitudes and the energy losses at high latitudes vary between 9.5 and 9.3 PW (Table 9 and Figure 13), which differ from the horizontal transports by only a few per cent. The origin of the adjustments to *TEI* reflects the imbalances of energy at the surface and TOA discussed in previous sub-sections. In ERA-Interim, the adjustments are dominated by those at the surface whereas in ERA-40 the adjustments come from both the surface and TOA. It is interesting that some of the energy inputs and losses at the surface are negative (Figure 13), which is probably indicative of the problems with the surface energy balance, rather than indicating that the signs should be reversed in reality. Given the problems with the energy balances at the TOA and surface, the adjusted energy inputs and losses (Table 9 and Figure 13) should not be considered too reliable.

5 Angular momentum

The axial component of the angular momentum of the atmosphere, *AM*, is a fundamental physical property of the atmosphere because its evolution in time is governed simply by the action of the torques exerted by frictional drag, in the boundary layer and due to the effects of gravity waves, T_F, and the mountain torque, T_M, involving the interaction of mountains and surface pressure, (Starr 1948). Furthermore, it is an interesting quantity to study because its variations are anti-correlated with the length of day (Hide et al 1980, Rosen and Salstein 1983). We write

$$AM = \frac{1}{g}\int dS \int_0^1 (a\cos(\varphi)u + \Omega a^2 \cos^2(\varphi))\frac{\partial p}{\partial \eta} d\eta \tag{11}$$

$$\frac{dAM}{dt} = T_M + T_F \tag{12}$$

$$T_M = -\frac{1}{g}\int p_S \frac{\partial \Phi_S}{\partial \lambda} dS \tag{13}$$

$$T_F = -\int a\cos(\varphi)\tau dS \tag{14}$$

where φ, u, Ω , p_s and τ are the latitude, zonal wind, angular rotation rate of the earth, surface pressure and the zonal component of frictional stress. The integral over S represents horizontal integration over the whole globe. Note that the angular momentum is a function of the global distribution of zonal winds and surface pressure according to (11). Here, the frictional torque is calculated from the (12 hour accumulated) forecast stress whereas the mountain torque is calculated from the four times daily analysed instantaneous surface pressure. We also note that this poor temporal sampling of the

mountain torque will introduce an error and it also means that the budget residual (*AM* tendency - the total torque) is not strictly proportional to the analysis increment, though a small residual should still be indicative of high quality data.

The mean annual cycle for the analysed global *AM*, whose peak to peak range is about 0.5% of the annual climate value of 1031×10^{25} kgm^2s^{-1}, reaches a maximum in December and a minimum in July (Table 10). The agreement between ERA-Interim and ERA-40 is good. The monthly mean anomalies of *AM* for the two ERA datasets also show a good correspondence (Figure 14a) and are quite stable with no large trends. The standard deviation of the anomalies and linear trends for *AM* in ERA-Interim for the period 1989-2008 are 1.1×10^{25} kgm^2s^{-1} and -0.5×10^{25} $kgm^2s^{-1}decade^{-1}$ while in ERA-40 for the period 1989-2001 they are 1.1×10^{25} kgm^2s^{-1} and -1.0×10^{25} $kgm^2s^{-1}decade^{-1}$ respectively, which are small compared to the global *AM* of the atmosphere. The annual climate value of *AM* has a contribution of 1016×10^{25} kgm^2s^{-1} from the surface pressure term and 15×10^{25} kgm^2s^{-1} from the zonal wind term. The standard deviations for the wind term, however, are at least three times greater than those for the surface pressure term. The most notable events in the *AM* anomaly time series are the temporary increase in *AM* by about 3×10^{25} kgm^2s^{-1} concurrent with the increase in the Nino3.4 SST index associated with the 1997-1998 El Niño, and in the late 1990s there is also a shift to slightly lower values.

As a consequence of the small trends and standard deviation in *AM*, its tendency (Figure 14b), calculated from the analysed values of *AM* at the beginning of each month, is small on average. The average torque, on the other hand, is much larger in magnitude, with an average value of -6 and -14 Hadleys for ERA-Interim and ERA-40 respectively (Figure 14c). This implies a loss of angular momentum during the 12 hour forecasts. The angular momentum budget residual does not oscillate about zero as it should, though it is much smaller and less variable in ERA-Interim than in ERA-40 (Figure 14d), indicating an improvement in data quality in the former. Furthermore, the residuals also improve with time (decrease towards zero) in both reanalyses, so that by 2006 the values in ERA-Interim are generally below 5 Hadleys. Again, this increase in quality with time is assumed to be indicative of the effects of the improving observing system and is associated with an increase of the torque over time (Figure 14c) rather than a large change in the analysed angular momentum tendency (Figure 14b). In the period 2006 to 2008 compared with 1989 to 1998 the total torque is 58% larger, the mountain torque is 34% smaller, the boundary layer frictional torque is 60% larger and the gravity wave drag frictional torque is 12% larger.

So it would appear that the improvement in time of the angular momentum budget residual (which is approximately proportional to the analysis increment) is dominated by an increase in the torque due to the boundary layer frictional drag. This could be effected either by a reduction in the drag on surface westerlies or an increase of the drag on surface easterlies. However, more subtle changes in the analysed angular momentum, mountain torque and torque due to gravity wave drag may still be important in improving the budget residual.

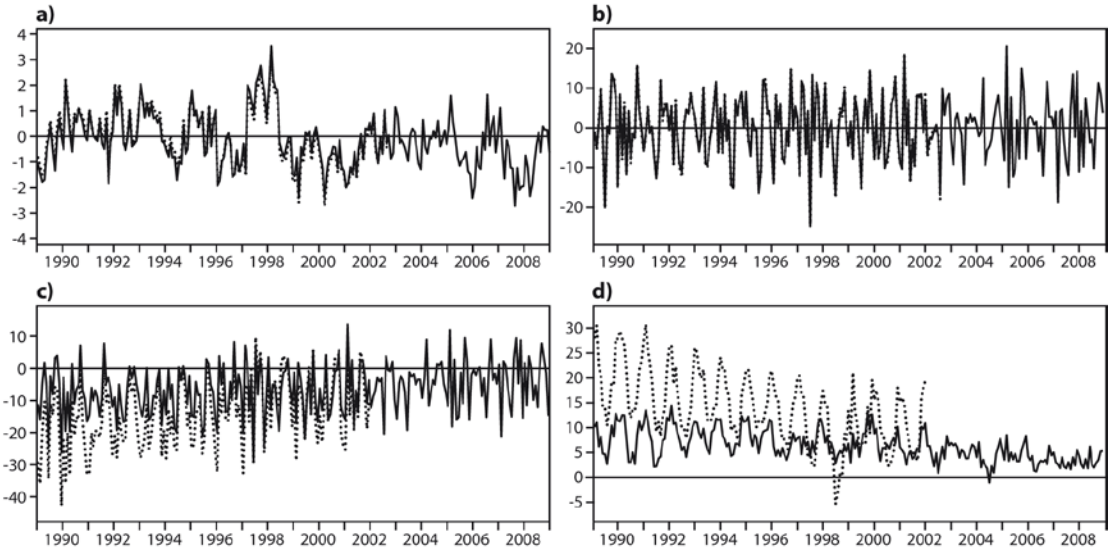

Figure 14: Monthly mean time series from 1989 to 2008 for ERA-Interim (solid) and ERA-40 (dashed) of a) analysed angular momentum (AM) anomaly, b) angular momentum tendency, c) torque and d) angular momentum budget residual (tendency – torque). The units in a) are 10^{25} kgm^2s^{-1} otherwise they are Hadleys (10^{18} Nm). The reference period in a) is 1989-2001.

	EI 20	EI 13	E4 13
Jan	1031.5	1031.5	1031.7
Feb	1031.4	1031.4	1031.7
Mar	1031.4	1031.7	1032.0
Apr	1032.0	1032.2	1032.6
May	1031.9	1032.0	1032.3
Jun	1029.2	1029.5	1029.7
Jul	1027.2	1027.2	1027.5
Aug	1027.4	1027.6	1027.9
Sep	1028.9	1029.0	1029.2
Oct	1031.1	1031.3	1031.6
Nov	1032.2	1032.5	1032.8
Dec	1032.3	1032.5	1032.8
Ann	1030.5	1030.7	1031.0
Max-min	5.0	5.3	5.4

Table 10: Mean annual cycle of angular momentum (AM) in ERA-Interim (EI) and ERA-40 (E4) for the 20 year period 1989-2008 and 13 year period 1989-2001. The units are 10^{25} kgm^2s^{-1}.

6 Summary and conclusions

In this work we have studied the atmospheric properties of mass, moisture, energy and angular momentum in ERA-Interim and compared them with those in ERA-40. These variables were chosen because they are governed by simple physical constraints. However, neither the ERA forecast model or assimilation system are designed to satisfy these physical constraints so the degree to which the reanalyses do so provides one measure of the quality of the data. Most of the measures used here indicate that the ERA-Interim reanalysis is superior in quality to ERA-40.

For ERA-Interim during 1989-2008 the standard deviation of the monthly mean global dry mass from the annual climate is 0.7 kgm^{-2} (0.07 hPa) or 0.007% and in ERA-40 for 1989-2001 it is 0.6 kgm^{-2} (0.06 hPa) or 0.006%. Although this indicates that global mass conservation is good, there has been a deterioration compared with ERA-40, though conservation in the mean annual cycle is better. There are spurious long time scale variations evident in dry mass, which are particularly pronounced in ERA-Interim and which originate predominately in the surface pressure field.

It has long been known that one of the greatest sources of uncertainty in atmospheric analyses originates in the divergent wind or mass flux (Boer and Sargent 1985), and ERA-Interim analyses are no exception. In particular, the hemispheric dry mass divergence, or cross equatorial mass flux, is not well analysed in ERA-Interim. This occurs because divergent winds and tropical winds, and in particular the meridional component of tropical winds (B.J. Hoskins pers. comm. 2009), are not well balanced and so are not constrained by the many satellite and synoptic observations of radiances, pressure and temperature. Graversen *et al.* (2007) speculated that the mass can be well analysed while the mass fluxes are not, because the forecast model moves the surface pressure towards the model's own climate by means of spurious mass fluxes which, unlike for surface pressure, are not corrected by the assimilation of observations. However, there has been a considerable improvement in the representation of the cross equatorial dry mass flux, or hemispheric dry mass divergence, on going from ERA-40 to ERA-Interim. This is thought to be mainly due to the use in ERA-Interim of 4D-Var data assimilation which should contribute to better time consistency than the 3D-Var used in ERA-40, though the homogenised radiosonde data (Haimberger 2007) and VarBC of satellite radiances (Dee and Uppala 2009) used in ERA-Interim may also be important. Furthermore, there appears to be an improvement in these divergent winds with time in ERA-Interim (but apparently not in ERA-40), a fact which is presumably due to the improving observing system and the ability of the 4D-Var in ERA-Interim to take advantage of it. Another measure of the improvement of the divergent winds is that the global standard deviation of the time mean divergence of dry mass flux, or budget residual, in ERA-Interim, of 10 $kgm^{-2}day^{-1}$, is less than half the value of 25 $kgm^{-2}day^{-1}$ in ERA-40.

Although far better than in ERA-40, moisture is still problematic in ERA-Interim. The global *E-P* in ERA-Interim has a temporal variation about 3 times larger than the *TCWV* tendencies and there are long periods of several years when *E-P* is either predominantly positive or negative which is related to changes in the observing system, such as the satellite measurements of *TCWV* from SSM/I (Dee *et al.* 2011). It has not been found necessary to mass adjust the moisture divergence in ERA-Interim where, for 1989-2008, the global time averaged moisture budget residual and its standard deviation is 0.003 $kgm^{-2}day^{-1}$ and 0.3 $kgm^{-2}day^{-1}$. In ERA-40 for 1989-2001 the values of 0.5 $kgm^{-2}day^{-1}$ and 1.1 $kgm^{-2}day^{-1}$ are much larger.

The net effect of the hydrological cycle in the atmosphere is to evaporate water from the oceans and transport it to land where it is rained out. We have used this idea to give us a simple physical measure of how well the moisture divergence and *E-P* fields match. Each of these three processes should involve the same amount of water. So, the integral of *E*-P over ocean should equal the atmospheric transport of *TCWV* from ocean to land (the integral of moisture divergence over ocean) which in turn should equal the integral of *P-E* over land. In ERA-Interim for 1989-2008 the transport of 1.1 Tgs^{-1} is weaker than the oceanic *E-P* and land *P-E* of 1.2 Tgs^{-1}. The precipitation over land in ERA-Interim for 1989-2008 (2.25 $kgm^{-2}day^{-1}$) is 5% larger than that from GPCP, see Simmons *et al*. (2010) for detailed comparisons with observations. Over oceans, however, the difference is greater (Dee *et al*. 2011) with ERA-Interim values (3.14 $kgm^{-2}day^{-1}$) being 9% larger than those in GPCP. If these observations are reliable and the transport is considered to be realistic, then the ERA-Interim evaporation over the ocean (3.43 $kgm^{-2}day^{-1}$) must be 9% too large. However, Trenberth *et al*. (2007) estimated the average transport of water from ocean to land to be 1.3 Tgs^{-1}, in which case, assuming GPCP to be correct, the ERA-Interim evaporation over land (1.53 $kgm^{-2}day^{-1}$) would be 9% too strong and over ocean it would be 8% too strong.

The TOA time averaged global energy losses are much improved in ERA-Interim compared to ERA-40, with values of 1 and 8 Wm^{-2} respectively. However, the opposite is true at the surface where the values are 7 and 4 Wm^{-2}. At the surface over land however, the energy loss of 0.5 Wm^{-2} in ERA-Interim is 0.8 Wm^{-2} smaller than that in ERA-40. The largest discrepancies in the global energy flows (Figure 8) between ERA-Interim and ERA-40 are in the solar radiation at the TOA and surface, which probably originates in changes to the clouds. Furthermore, Kållberg (2011) speculated that the spin-up of cloud in the ERA-Interim forecast model is responsible for the spin-down of the surface energy losses and spin-up of the TOA energy losses. We have also compared the TOA annual climate of radiative fluxes in ERA-Interim with those from adjusted CERES data and found similar deficiencies to those found by Trenberth and Fasullo (2010) for reanalyses including ERA-40 and JRA-25. They found that the problems originated in too bright clouds over tropical oceans, too little cloud over low latitude land and too little cloud over higher latitudes, particularly over the Southern Ocean. So it would seem that ERA-Interim still suffers from various problems due to the misrepresentation of clouds.

TFK09 discussed the current uncertainty in the downwelling thermal radiation at the surface (STRD). They estimated this quantity to be 333 Wm-2 while other estimates quote values of 340 Wm^{-2} or higher. The value in ERA-Interim is towards the higher end of these estimates, being 341 Wm^{-2}. However, as already noted, deficiencies exist in ERA-Interim, particularly in the clouds, which have a large influence on STRD.

In ERA-Interim for 1989-2008 the global average of the time averaged mass adjusted energy budget residual is 8 Wm^{-2} and the global standard deviation is 11 Wm^{-2}. In ERA-40 for 1989-2001 the balance is much poorer over much of the globe with the average of the residual being 11 Wm-2 and the standard deviation 25 Wm^{-2}. The standard deviations of the residuals using the unadjusted divergence are larger, with values of 38 and 95 Wm-2 in ERA-Interim and ERA-40 respectively. So even though the problem is not as accute in ERA-Interim as in ERA-40, it is still necessary to mass adjust energy fluxes and their divergence in both reanalyses. Regardless of whether or not the energy divergences are mass adjusted, the energy budget residuals, which are proportional to the analysis increments for

energy, are smaller in ERA-Interim than those in ERA-40. The energy increments in ERA-Interim vary on long timescales, as also found by Chiodo and Haimberger (2010).

The net effect of the energy cycle of the atmosphere is that energy is absorbed at the TOA at low latitudes, some of which is lost to the surface while the remainder is transported to high latitudes which then, augmented by energy from the surface, is lost to space (Figure 13). We have used this idea to give us a simple physical measure of how well the energy divergence and TEI fields match. The difference between the energy in at the TOA and out at the surface at low latitudes should match the energy transport from low to high latitudes (the integral of divergence of energy fluxes over low latitudes) which, in turn, should match the difference between the energy out at the TOA and in at the surface at high latitudes.

The mass adjusted horizontal atmospheric energy transports of 9.5 and 9.3 PW (the unadjusted transports are 10.3PW) for ERA-Interim and ERA-40 respectively (Figure 13) are similar to the sum of the peak atmospheric energy transports from both hemispheres (about 5 PW in each) given by Trenberth and Carron (2001) and Fasullo and Trenberth (2008b). However, the horizontal transports are weaker than the energy losses at high latitudes and much larger than the energy inputs at low latitudes. The mismatches between the three processes can be reduced to just a few per cent by making simple global adjustments to *TEI*. However, given the problems with the energy balances at the TOA and surface, the adjusted energy inputs and losses should not be considered too reliable. We saw in Section 4.2 that compared with CERES data, the meridional gradient of R_T in ERA-Interim is too weak. If R_T were to be made compatible with CERES data, then the low latitude energy input would have to be increased by 17% and the energy loss from high latitudes would have to be increased by 12%. This either implies that the adjusted atmospheric energy transports are at least 10% too weak or that the globally adjusted F_S is too weak.

The angular momentum budget residuals, which are approximately proportional to the analysis increments, in ERA-Interim are smaller than in ERA-40. Furthermore, these residuals decrease with time in both ERA-Interim and ERA-40, presumably because of the improving observing system.

We have seen that the analysis increments for both energy and angular momentum are smaller in ERA-Interim than in ERA-40. For the case where there are very few observations and/or very poor observations, small analysis increments (which indicate the change in the variable from the forecast to the analysis due to the assimilation of observations) would indicate that the forecast state is close to the analysed state because the observations are unable to change the analysis significantly. However, in ERA-Interim there is a good supply of high quality observations and ERA-Interim analyses and forecasts are known to be more consistent with observations than was ERA-40 (Simmons et al. 2007, Uppala et al. 2008 and Dee et al. 2011). In this case, the smaller analysis increments are usually thought to indicate an improvement in both the analyses and associated forecasts.

Acknowledgments

We would like to thank many of the staff of the ECMWF for enabling this work to be carried out, but Jean-Jacques Morcrette and Agathe Untch deserve particular thanks, as do Rob Hine and Anabel Bowen for cleaning up the figures and creating Figure 13. We would also like to thank Kevin Trenberth and one anonymous reviewer for making helpful suggestions on improving this work. PB is funded by NCAS-Climate and HS is funded by JMA.

References

Adler, R. F., et al., 2003: The Version 2 Global Precipitation Climatology Project (GPCP) monthly precipitation analysis (1979-present). *J. Hydromet*., **4**, 1147-1167.

Bannon, P. R., C. H. Bishop and J. B. Kerr, 1997: Does the surface pressure equal the weight per unit area of a hydrostatic atmosphere. *Bull. Amer. Meteor. Soc*., **78**, No. 11, 2637-2642.

Berrisford, P., D. Dee, K. Fielding, M. Fuentes, P. Kallberg, S. Kobayashi and S. Uppala, 2009: The ERA-Interim archive. *ERA report series*, 1, pp 16. (see http://www.ecmwf.int/publications/)

Boer, G. J., 1982: Diagnostic equations in isobaric coordinates. *Mon. Wea. Rev*., **110**, 1801-1820.

Boer, G. J. and N. E. Sargent, 1985: Vertically integrated budgets of mass and energy for the globe. *J. Atmos. Sci.*, **15**, 1592-1613.

Chiodo, G., and L. Haimberger, 2010: Interannual changes in mass consistent energy budgets from ERA-Interim and satellite data. *J. Geophys. Res*., **115**, pp 22.

Dee, D. and S. Uppala, 2009: Variational bias correction in ERA-Interim. *Q. J. R. Meteorol. Soc*., **135**, 1830-1844.

Dee, D. et al., 2011: The ERA-Interim reanalysis: configuration and performance of the data assimilation system. *Q. J. R. Meteorol. Soc*., **137**, 553-597.

Fasullo, J. T. and K. E. Trenberth, 2008a: The annual cycle of the energy budget. Part I: Global mean and land-ocean exchanges. *J. Climate*, **21**, 2297-2312.

Fasullo, J. T. and K. E. Trenberth, 2008b: The annual cycle of the energy budget. Part II: Meridional structures and poleward transports. *J. Climate*, **21**, 2313-2325.

Graversen, R. G., E. Källén, M. Tjernström and H. Körnich, 2007: Atmospheric mass-transport inconsistencies in the ERA-40 reanalysis. *Q. J. R. Meteorol. Soc*., **133**, 673-680.

Gibson, J. K., P. Kållberg, S. Uppala, A. Nomura, A. Hernandez and E. Serrano, 1997: ERA description. *ERA-15 project report series*, 1, pp 72. (see http://www.ecmwf.int/publications/)

Haimberger, L., 2007. Homogenization of radiosonde temperature time series using innovation statistics. *J. Climate*, **20**, 1377-1403.

Haimberger, L., B. Ahrens, F. Hamelbeck and M. Hantel, 2001: Impact of time sampling on atmospheric energy budget residuals. *Meteorol. Atmos. Phys*., **77**, 167-184.

Hide, R., N. T. Birch, L. V. Morrison, D. J. Shea and A. A. White, 1980: Atmospheric angular momentum fluctuations and changes in the length of the day. *Nature*, **286**, 114-117.

Kållberg, P., 2011: Forecast drift in ERA-Interim. *ERA report series* No.11, pp 9. (see http://www.ecmwf.int/publications/)

Kållberg, P., A. J. Simmons, S. Uppala and M. Fuentas, 2004: The ERA-40 archive. *ERA-40 project report series*, 17, pp 31. (see http://www.ecmwf.int/publications/)

Kållberg, P., P. Berrisford, B. J. Hoskins, A. J. Simmons, S. Uppala, S. Lamy-Thepaut and R. Hine, 2005: ERA-40 atlas. *ERA-40 project report series*, 19, pp 191.

Kistler, R., et al, 2001: The NCEP-NCAR 50-year reanalysis: Monthly means CD-Rom and documentation. *Bull. Am. Meteorol. Soc.*, **82**, 247-267.

Lott, F., A. W. Robertson and M. Ghil, 2004: Mountain torques and Northern Hemisphere low-frequency variability. Part I: Hemispheric aspects. *J. Atmos. Sci*., 61, 1259-1271.

Onogi, K., et al, 2007: The JRA-25 reanalysis. *J. Meteor. Soc. Japan*, **85**, 369-432.

Sardeshmukh, P. D. and B. J. Hoskins, 1984: Spatial smoothing on the sphere. *Mon. Wea. Rev*., **112**, 2524-2529.

Rosen, R. and D. Salstein, 1983: Variations in atmospheric angular momentum on global and regional scales and the length of day. *J. Geophys. Res.*, **88**, 5451-5470.

Simmons, A. J. and D. M. Burridge, 1981: An energy and angular momentum conserving vertical finite difference scheme and hybrid vertical coordinates. *Mon. Wea. Rev*., **109**, 758-766.

Simmons, A., S. Uppala, D. Dee and S. Kobayashi, 2007: ERA-Interim: New ECMWF reanalysis products from 1989 onwards. *ECMWF Newsletter*, **110**, 25-35.
(see http://www.ecmwf.int/publications/newsletters/)

Simmons, A. J., K. M. Willett, P. D. Jones, P. W. Thorne and D. P. Dee, 2010: Low-frequency variations in surface atmospheric humidity, temperature, and precipitation: Inferences from reanalyses and monthly gridded observational data sets. *J. Geophys. Res*., **115**, pp 21.

Trenberth, K. E., 1981: Seasonal variations in global sea level pressure and the total mass of the atmosphere. *J. Geophys. Res*., **86**, 5238-5246.

Trenberth, K. E., 1991: Climate diagnostics from global analyses: conservation of mass in ECMWF analyses. *J. Climate*, **4**, 707-722.

Trenberth, K. E., and C. J. Guillemot, 1994: The total mass of the atmosphere. *J. Geophys. Res*., **99**, 23 079-23 088.

Trenberth, K. E., and A. Solomon, 1994: The global heat balance: Heat transports in the atmosphere and ocean. *Climate Dyn*., **10**, 107-134.

Trenberth, K. E., and J. M. Caron, 2001: Estimates of meridional atmosphere and ocean heat transports. J. *Climate*, **14**, 3433-3443.

Trenberth, K. E., and L. Smith, 2005: The Mass of the Atmosphere: A constraint on Global Analyses. *J. Climate*, **18**, 864-875.

Trenberth, K. E., and L. Smith, 2009: The three dimensional structure of the atmospheric energy budget: Methodology and evaluation. *Climate Dyn*., **32**, 1065-1079.

Trenberth, K. E., and J. T. Fasullo, 2010: Simulation of present-day and twenty-first-century energy budgets of the Southern Oceans. *J. Climate*, **23**, 440-454.

Trenberth, K. E., L. Smith, T. Qian, A. Dai and J. Fasullo, 2007: Estimates of the global water budget and its annual cycle using observational and model data. *J. Hydromet*., **8**, 758-769.

Trenberth, K. E., J. T. Fasullo and J, Kiehl, 2009; Earth's global energy budget. *Bull. Amer. Meteor. Soc*., **90**, No. 3, 311-324, doi:10.1175/2008BAMS2634.1.

Uppala, S.M., et al, 2005: The ERA-40 reanalysis. *Q. J. R. Meteorol. Soc*., **131**, 2961-3012.

Uppala, S., D. Dee, S. Kobayashi, P. Berrisford and A. Simmons, 2008: Towards a climate data assimilation system: status update of ERA-Interim. *ECMWF Newsletter*, 115, 12-18.
(see http://www.ecmwf.int/publications/newsletters/)

Zhao, Y. and J. Li, 2006: Discrepancy of mass transport between the Northern and Southern Hemispheres among the ERA-40, NCEP/NCAR, NCEP-DOE AMIP-2 and JRA-25 reanalysis. *Geophys. Res. Lett*., **33**, pp 5.